CHAPTER 4

Geochemistry

Geochemical composition can be divided by volume into major oxides, minor elements, trace elements and rare earth elements. These chemical compositions, especially immobile incompatible elements, can be used for identification of rock types and determining magma characteristics because they are closely representative of magma. Moreover, the chemical compositions will provide for interpretation of tectonic setting by using discrimination diagram and comparison with modern magma suites.

The studied volcanic and associated rocks have experiences variable degrees of alteration and/or metamorphism. The mobile elements (Rollison, 1993) commonly will take place during weathering, diagenesis and metamorphism or through interaction with a hydrothermal fluid. Consequently, the chemical compositions of the studied rocks are unlikely to represent the primary compositions derived from magma. The concentrations of some major elements in ancient igneous rocks are easily to removing during magmatic evolution. However, it is generally agreed that Fe_2O_3, FeO and MgO are slightly removed from primary values. Trace element mobility (Rollinson, 1993) is controlled by the mineral changes which occurred during alteration and nature of fluid phase. The incompatible elements which belong to the low field strength elements (LFSE) group are mobile, whereas the high field strength elements (HFSE) Ti, Zr, Y, Nb, Ta, Th and P, and also transitional elements Ni, Cr, V and Sc are immobile. The concentrations and the ratios of the immobile elements remain constant in both unaltered and altered rocks. In addition, Zr is an immobile incompatible elements (Green, 1980) used as a fractionation parameter for the studied rock samples. Also, occasion reports have appeared rare earth elements (REE), especially light rare earth elements (LREE), mobility during hydrothermal alteration and low grade metamorphism (Hellman and Henderson, 1979; Whiterford *et al*., 1988), so, the REE patterns of carefully selected samples are probably slightly shifted from their primary patterns, but remain parallel/subparallel to the primary patterns.

4.1 Sample Preparation

Carefully and avoid select the rock samples that have secondary minerals and more alteration based on petrography data by polarizing microscope checking to obtain least-altered samples. All of those should avoid as follow;

1) full of alteration product of primary mineral of each rocks. For example, plagioclase alter to sericite and/ or mafic minerals alter to serpentine/ chlorite;

2) abundant of secondary minerals replacement such as quartz, epidote, carbonates, Fe-oxide, and chlorite;

3) extensive of vesicles, amygdales, xenocrysts and xenoliths;

4) well-developed foliation and other metamorphism; and

5) permeated with veined minerals such as epidote, quartz and calcite and /or patches totally more than approximately 5 modal %

The least-altered 30 samples were selected and done for powder samples to measure for whole-rock chemistry. These powder samples were chemically analyzed for major oxides, trace elements and loss on ignition (LOI). The representatives of the least-altered samples were analyzed for rare-earth elements (REE).

The analyzed powder samples were carefully prepared by cutting off the weathering surfaces of the least-altered samples, and then splitting them into conveniently sized fragments and crushing them into small chips (approximately 5 mm across) using Rocklabs Hydraulic Splitter and Jaw Crusher. After that, the rock chips were selected to avoid veins, vesicles, amygdales, xenecrysts, xenoliths and weathering surfaces, and were cleaned to make powder samples. The cleaned rock chips were divided by quartering them into 50-80 g pieces and then were pulverized by Rocklabs Tungsten Carbide Ring Mill to be powder samples. The powder samples were prepared at the Department of Geological Sciences, Chiang Mai University, Thailand.

4.2 Analytical Techniques

4.2.1 Major Oxides and Trace Elements Analysis

The chemical analysis of major oxides (SiO_2, TiO_2, Al_2O_3, Fe total as Fe_2O_3, MnO, MgO, CaO, Na_2O, K_2O and P_2O_5) and trace elements (Rb, Sr, Zr, Y, Nb, Ni, Cr, V and Sc) were made up by a Phillip-MagixPro PW 2400 Wavelength Dispersive X-Ray Fluorescence (XRF) Spectrometer, fixed at the Department of Geological Sciences, Chiang Mai University. The instrumental parameters consist of a Rhodium tube with a lithium fluoride 200 crystal (used in an elemental range of K-Ru), and scintillation and flow proportion detectors, and X-ray tube operated at 60 kV with a current of up to 125 mA; at a maximum power level of 4 kW. The net (background corrected) intensities were measured, subsequently, calculated against the calibrations derived from 7 international standard reference materials (AGV-2, BCR-2, BHVO-2, BIR-1, DNC-1, GSP-2 and W-2). The inter-elements matrix corrections were done by the Super Q version 3.0 program. The reporting detection limit is about 0.001% for major oxides and 3 ppm for trace elements. The accuracy and precision for most of the elements are better than 5%.

The major oxides analysis was measured from fusion disc samples. Fusion disc was done by mixing 0.8 g powder sample with 0.06 g lithium bromide (LiBr) and 4.0 g di-lithium tetraborate ($Li_2B_4O_7$) in a platinum crucible. The mixture was fused by burners, and then cooled down in a 3 cm platinum mold. The trace element analysis was measured from pressed powder (pellet) by mixing 5.0 g powder sample with 0.3 g wax ($C_6H_8O_3N_2$) in an aluminum cup filled by 3.0 g boric acid (H_3BO_3), and then pressed by a hydraulic machine at 200 kN for 1 minute.

4.2.2 Loss on Ignition Determination

Loss on ignition (LOI) was analyzed by heating a platinum crucible contained 1.0 g sample in a furnace at 1000ºC for 12 hours at the Department of Geological Sciences, Chiang Mai University. Powder sample approximately 1.0 g must be weighed before and after heating for calculating LOI.

4.2.3 Rare Earth Element Analysis

The 16 least-altered samples were selected for low abundance trace elements (Hf, Th and Ta) and rare earth elements (La, Ce, Pr, Nd, Sm, Eu, Gd, Tb, Dy, Ho, Er, Tm and Yb) analyses using a Sodium Peroxide Fusion combined inductively coupled plasma atomic emission spectroscopy (ICP-AES) and inductively coupled plasma mass spectrometry (ICP-MS) methods at the Sgs-Cstc Standards Technical Services Co.,Ltd. in China.

This analysis was measured from digested sample solution. Weighted 0.1 g representative samples are digested fused in glassy carbon crucibles using sodium peroxide (Na_2O_2). The resultant cake is dissolved in HNO_3. The digested sample solution is analyzed by inductively coupled plasma Mass Spectrometer (ICP-MS) and inductively coupled plasma Optical Emission Spectrometer (ICP-OES). Computer, on line, data fed to SGS Laboratory Information Management System with secure audit trail.

The analytical results for major oxides, trace elements, REE, Ta and Hf analysis of the studied volcanic and associated samples are reported in Table 4.1.

4.3 Magmatic Affinities of Volcanic and Associated Rocks

The representatives of volcanic and associated rocks presented in this study show different types of REE patterns, N-MORB normalized multi-element patterns and variation diagram. Using these mutli-element patterns, the studied rocks can be separated into 8 magmatic groups. These studied rocks are distributed in rhyolite, rhyodacite/ dacite, andesite, andesite/ basalt, sub-alkaline basalt, and alkali basalt fields in Zr/TiO_2 vs. Nb/Y diagram (Winchester and Floyd, 1977) (Figure 4.1).

4.3.1 Group I Rocks

The Group I rocks (sample number BTK25/1-1, BTK25/1-2, and BTK 25/7) were collected from the Mae Phrik area, and are rhyodacite. They have Zr/TiO_2 against Nb/Y ratios in ranges of 0.0631-0.0809 and 0.1120-0.1631, respectively, corresponding subalkalic series (Figure 4.1).

Table 4.1 Whole-rock analyses for major oxides on volatile-free basis, trace elements, loss on ignition, rare earth elements and some selected ratios of the studied least-altered volcanic and associated rocks.

	Mae Phrik area					Mae Salaem area
Sample	BTK25/1-1	BTK25/1-2	BTK25/7	BTK25/8-1	BTK25/8-3	MSL25/1-1
Major oxides (wt%)						
SiO_2	74.23	77.01	72.62	60.19	49.86	76.09
TiO_2	0.23	0.23	0.37	0.92	1.82	0.07
Al_2O_3	12.47	12.73	12.61	17.13	18.89	12.26
Fe_2O_3tt	2.48	3.38	3.38	4.91	8.28	1.36
MnO	0.03	0.02	0.08	0.09	0.13	0.06
MgO	0.45	0.58	0.69	6.05	8.32	0.07
CaO	1.73	0.08	2.11	0.62	1.06	0.35
Na_2O	1.79	0.54	4.22	6.42	6.43	3.05
K_2O	2.12	2.47	0.95	0.04	0.06	4.86
P_2O_5	0.04	0.04	0.07	0.33	0.77	0.01
LOI	3.70	3.32	3.52	3.28	4.89	1.21
Original Sum	99.28	100.41	100.62	99.97	100.50	99.38
Trace elements (ppm)						
Ni	3.23	6.37	5.88	109.54	165.16	3.21
V	47.52	49.08	73.91	151.58	268.89	23.34
Rb	91.94	114.26	35.22	5.68	BD	232.41
Y	76.05	75.41	70.91	BD	BD	55.24
Nb	BD	BD	0.39	23.02	39.73	12.23
Hf		4	4		5	7
Th	2.71	2.21	7.01	46.51	54.52	54.57
Ta		2	1.4		1.1	2.4
Cr	10.38	3.86	3.03	184.32	616.87	1.36
Sr	63.08	61.61	92.06	171.82	75.42	107.24
Ba	909.89	982.09	729.10	498.68	331.03	840.02
Sc	6.53	0.42	9.76	1.44	3.50	2.79
Zr	198.66	191.84	243.35	198.48	326.42	166.12
Rare Earth elements (ppm)						
La		15.60	20.90		295.00	40.50
Ce		32.70	39.30		488.00	65.90
Pr		4.64	5.47		50.18	7.01
Nd		21.10	23.50		158.00	24.30
Sm		3.90	5.50		18.60	4.00
Eu		1.17	1.40		1.92	0.49
Gd		4.20	5.72		16.70	3.73
Tb		0.77	1.12		1.13	0.57
Dy		5.45	6.60		3.92	3.11
Ho		1.32	1.51		0.69	0.70
Er		3.81	4.16		2.33	1.90
Tm		0.73	0.82		0.35	0.39
Yb		4.10	4.70		2.40	2.50
Lu		0.77	0.86		0.53	0.42
Selected element ratios						
Ti/Zr	7.07	7.23	9.20	27.79	33.48	2.47
Zr/Nb			623.97	8.62	8.22	13.58
Zr/Y	2.61	2.54	3.43			3.01
Nb/Y			0.01			0.22
$[La/Sm]_{cn}$		2.44	2.32		9.67	6.17
$[Sm/Yb]_{cn}$		1.03	1.27		8.40	1.73

BD = below detection limite.
cn=chondrite-normalized values

Table 4.1 Continued

	Pong Daeng area			Wang Luek area		
Sample	PDNG30/4	WL29/1-1	WL29/1-2	WL29/1-3	WL29/2-1	WL29/2-2
Major oxides (wt%)						
SiO_2	49.95	48.43	47.28	46.15	48.19	51.85
TiO_2	1.09	0.36	0.56	1.46	0.43	0.99
Al_2O_3	18.29	20.05	18.31	16.38	17.43	16.47
Fe_2O_3tt	9.89	7.76	10.07	12.43	7.48	8.78
MnO	0.18	0.14	0.17	0.19	0.14	0.15
MgO	4.00	5.96	7.79	6.54	7.77	7.09
CaO	6.46	11.64	10.31	12.81	15.01	7.62
Na_2O	4.74	1.86	1.15	0.99	1.42	2.71
K_2O	0.12	0.20	0.29	0.08	0.11	0.09
P_2O_5	0.22	0.07	0.07	0.02	0.01	0.27
LOI	5.67	3.59	3.72	2.89	2.61	3.57
Original Sum	100.60	100.04	99.73	99.95	100.60	99.58
Trace elements (ppm)						
Ni	17.10	15.76	17.85	9.25	9.48	99.74
V	165.80	63.18	83.70	227.44	72.68	139.82
Rb	10.05	10.75	12.64	8.45	8.53	8.49
Y	29.46	7.84	5.52	6.11	6.02	19.34
Nb	2.85	0.73	2.06	1.49	0.99	7.07
Hf	5	2				5
Th	5.45	0.10	1.32	2.12	0.40	6.02
Ta	1	0.4				1.8
Cr	24.59	127.50	184.02	271.72	64.36	349.21
Sr	668.91	366.54	297.43	336.65	318.26	387.41
Ba	550.87	658.91	630.38	433.80	636.67	538.44
Sc	18.55	31.75	30.44	35.58	41.16	23.53
Zr	152.18	48.45	42.85	48.80	45.27	136.29
Rare Earth elements (ppm)						
La	17.20	3.10				20.50
Ce	32.10	5.20				39.90
Pr	4.39	0.74				5.28
Nd	18.70	3.20				21.70
Sm	4.50	0.90				4.10
Eu	1.36	1.10				1.25
Gd	4.33	0.66				3.87
Tb	0.72	0.10				0.65
Dy	4.24	0.78				3.35
Ho	0.95	0.18				0.71
Er	2.57	0.49				1.78
Tm	0.46	0.10				0.33
Yb	2.60	0.60				1.80
Lu	0.44	0.09				0.29
Selected element ratios						
Ti/Zr	42.79	44.46	77.83	179.36	56.85	43.69
Zr/Nb	53.40	66.37	20.80	32.75	45.73	19.28
Zr/Y	5.17	6.18	7.76	7.99	7.52	7.05
Nb/Y	0.10	0.09	0.37	0.24	0.16	0.37
$[La/Sm]_{cn}$	2.33	2.10				3.05
$[Sm/Yb]_{cn}$	1.88	1.63				2.47

BD = below detection limite.
cn=chondrite-normalized values

Table 4.1 Continued

	Wang Luek area		Wang Prachop area			
Sample	WL29/3	WPC26/3-1	WPC26/4	WPC26/7	WPC26/10	WPC26/11
Major oxides (wt%)						
SiO_2	47.97	80.11	57.69	60.30	57.28	57.47
TiO_2	1.24	0.05	0.87	0.69	0.85	0.86
Al_2O_3	16.94	12.40	17.51	16.16	16.24	16.43
Fe_2O_3tt	10.44	0.83	6.90	6.27	7.04	7.21
MnO	0.16	0.01	0.16	0.11	0.12	0.13
MgO	7.83	0.10	2.24	3.06	3.94	3.97
CaO	6.24	0.07	3.27	5.99	5.95	5.44
Na_2O	2.42	2.24	3.45	2.36	2.22	2.69
K_2O	2.46	2.69	4.67	2.26	2.67	2.21
P_2O_5	0.23	0.01	0.32	0.14	0.20	0.20
LOI	4.31	1.57	2.08	2.19	3.50	3.26
Original Sum	100.23	100.09	99.15	99.53	100.03	99.86
Trace elements (ppm)						
Ni	60.85	8.09	5.53	18.53	40.15	39.42
V	189.04	31.48	134.73	101.06	126.38	126.37
Rb	75.95	173.23	145.52	76.62	100.94	87.41
Y	38.77	75.90	74.48	48.00	46.38	44.57
Nb	3.01	6.02	6.57	5.91	6.76	5.73
Hf	3	3	4			
Th	1.47	25.58	6.58	8.25	7.33	6.75
Ta	1.4	1.5	1.6			
Cr	225.07	15.66	9.27	80.78	121.31	118.88
Sr	257.13	114.35	357.31	337.70	395.40	356.38
Ba	748.39	1533.07	1071.15	782.09	834.70	789.58
Sc	21.99	3.94	11.42	18.28	20.16	15.28
Zr	102.93	128.09	247.45	172.92	169.32	170.36
Rare Earth elements (ppm)						
La	7.50	14.70	26.30			
Ce	19.10	25.80	54.20			
Pr	3.08	3.96	7.33			
Nd	14.40	14.70	30.40			
Sm	3.30	2.80	5.50			
Eu	1.21	0.86	2.06			
Gd	3.31	3.01	6.09			
Tb	0.67	0.58	1.02			
Dy	3.68	3.78	6.00			
Ho	0.80	0.96	1.31			
Er	2.16	2.80	3.36			
Tm	0.39	0.50	0.63			
Yb	2.20	3.20	3.60			
Lu	0.36	0.53	0.64			
Selected element ratios						
Ti/Zr	71.99	2.55	20.99	23.86	30.21	30.41
Zr/Nb	34.20	21.28	37.66	29.26	25.05	29.73
Zr/Y	2.65	1.69	3.32	3.60	3.65	3.82
Nb/Y	0.08	0.08	0.09	0.12	0.15	0.13
$[La/Sm]_{cn}$	1.39	3.20	2.91			
$[Sm/Yb]_{cn}$	1.63	0.95	1.66			

BD = below detection limite.
cn=chondrite-normalized values

Table 4.1 Continued

	Wang Prachop area			Wang Chao area		
Sample	WPC26/12	WPC27/2	WPC27/3	WCH26/2-1	WCH26/2-2	WCH26/3-1
Major oxides (wt%)						
SiO_2	60.17	60.40	61.39	78.22	77.78	77.14
TiO_2	0.75	0.73	0.76	0.05	0.06	0.05
Al_2O_3	16.29	16.29	16.37	12.36	12.03	12.07
Fe_2O_3tt	6.52	6.34	5.98	0.32	0.53	0.85
MnO	0.11	0.12	0.14	0.01	0.01	0.02
MgO	2.74	3.01	2.91	0.02	0.02	0.12
CaO	5.37	3.73	2.84	0.06	0.06	0.32
Na_2O	2.57	2.58	5.50	2.59	1.88	3.26
K_2O	2.36	3.82	0.64	5.66	6.80	4.37
P_2O_5	0.17	0.16	0.17	0.01	0.00	0.00
LOI	2.56	2.74	3.40	1.05	1.08	1.22
Original Sum	99.60	99.92	100.09	100.34	100.26	99.42
Trace elements (ppm)						
Ni	17.93	11.47	7.14	8.55	2.60	8.28
V	112.90	108.44	116.84	20.72	21.46	20.64
Rb	87.43	133.79	32.93	386.84	466.07	427.34
Y	46.25	59.73	43.91	89.10	109.72	130.44
Nb	5.73	4.87	4.54	31.64	33.47	45.84
Hf	4		8			
Th	8.04	7.56	9.38	78.25	75.81	65.75
Ta	1.4		1.5			
Cr	54.77	59.91	48.63	2.52	2.69	23.27
Sr	318.69	331.52	335.50	104.70	105.95	94.75
Ba	781.50	1112.28	694.35	820.86	877.15	858.51
Sc	17.74	14.31	10.30	1.25	3.54	0.79
Zr	172.34	189.07	210.26	179.43	182.05	157.06
Rare Earth elements (ppm)						
La	24.70		28.70			
Ce	46.60		50.20			
Pr	6.08		6.92			
Nd	23.90		28.30			
Sm	4.20		4.90			
Eu	1.31		1.29			
Gd	4.60		5.34			
Tb	0.80		0.91			
Dy	4.36		4.97			
Ho	0.99		1.09			
Er	2.27		2.75			
Tm	0.40		0.50			
Yb	2.40		2.70			
Lu	0.44		0.51			
Selected element ratios						
Ti/Zr	26.03	23.06	21.59	1.65	1.92	2.00
Zr/Nb	30.08	38.82	46.31	5.67	5.44	3.43
Zr/Y	3.73	3.17	4.79	2.01	1.66	1.20
Nb/Y	0.12	0.08	0.10	0.36	0.31	0.35
$[La/Sm]_{cn}$	3.58		3.57			
$[Sm/Yb]_{cn}$	1.90		1.97			

BD = below detection limite.
cn=chondrite-normalized values

Table 4.1 Continued

	Wang Chao area					
Sample	WCH26/3-2	WCH26/4	WCH26/5	WCH27/5-2	WCH28/4	WCH28/8-1
Major oxides (wt%)						
SiO_2	76.94	78.07	78.33	72.79	62.52	53.47
TiO_2	0.05	0.05	0.13	0.31	0.78	1.56
Al_2O_3	13.09	11.98	12.47	13.66	16.53	17.93
Fe_2O_3tt	0.72	0.72	1.03	2.06	5.35	8.67
MnO	0.02	0.01	0.01	0.03	0.12	0.17
MgO	0.08	0.10	0.20	0.35	1.83	4.12
CaO	0.12	0.26	0.04	0.16	4.35	2.33
Na_2O	3.15	3.52	0.11	3.77	3.72	4.41
K_2O	4.68	4.01	6.09	4.84	1.92	1.46
P_2O_5	0.00	0.01	0.01	0.05	0.23	0.57
LOI	1.08	1.07	2.09	1.46	1.92	4.78
Original Sum	99.94	99.78	100.54	99.49	99.26	99.46
Trace elements (ppm)						
Ni	0.85	12.93	6.61	6.08	2.81	85.39
V	19.54	19.98	31.08	63.56	130.25	268.35
Rb	341.08	273.65	405.14	183.24	80.67	77.89
Y	110.87	95.04	106.75	83.16	44.95	42.96
Nb	30.94	27.45	20.52	17.46	6.73	14.00
Hf		5		5	4	2
Th	77.76	79.27	72.93	30.10	12.00	17.50
Ta		1.4		2.8	1.3	0.6
Cr	0.41	4.06	5.88	1.33	13.00	194.16
Sr	78.56	91.12	91.47	116.31	396.66	178.88
Ba	761.54	766.07	959.61	929.93	850.67	576.52
Sc	2.50	0.66	2.41	2.27	14.87	6.45
Zr	174.24	188.89	385.39	371.44	211.32	228.59
Rare Earth elements (ppm)						
La		17.20		38.50	29.80	40.80
Ce		27.50		71.30	55.90	69.90
Pr		5.69		9.05	6.86	10.78
Nd		24.60		33.80	27.00	43.90
Sm		6.50		5.00	5.60	6.90
Eu		0.27		1.22	1.62	2.33
Gd		6.24		5.32	4.60	6.91
Tb		1.22		0.98	0.83	0.94
Dy		6.77		5.54	4.21	5.35
Ho		1.40		1.21	0.89	1.06
Er		3.49		3.37	2.35	2.77
Tm		0.69		0.62	0.44	0.47
Yb		4.00		3.60	2.60	2.50
Lu		0.62		0.63	0.42	0.42
Selected element ratios						
Ti/Zr	1.77	1.57	1.97	5.02	21.99	40.81
Zr/Nb	5.63	6.88	18.78	21.27	31.40	16.33
Zr/Y	1.57	1.99	3.61	4.47	4.70	5.32
Nb/Y	0.28	0.29	0.19	0.21	0.15	0.33
$[La/Sm]_{cn}$		1.61		4.69	3.24	3.60
$[Sm/Yb]_{cn}$		1.76		1.50	2.33	2.99

BD = below detection limite.
cn=chondrite-normalized values

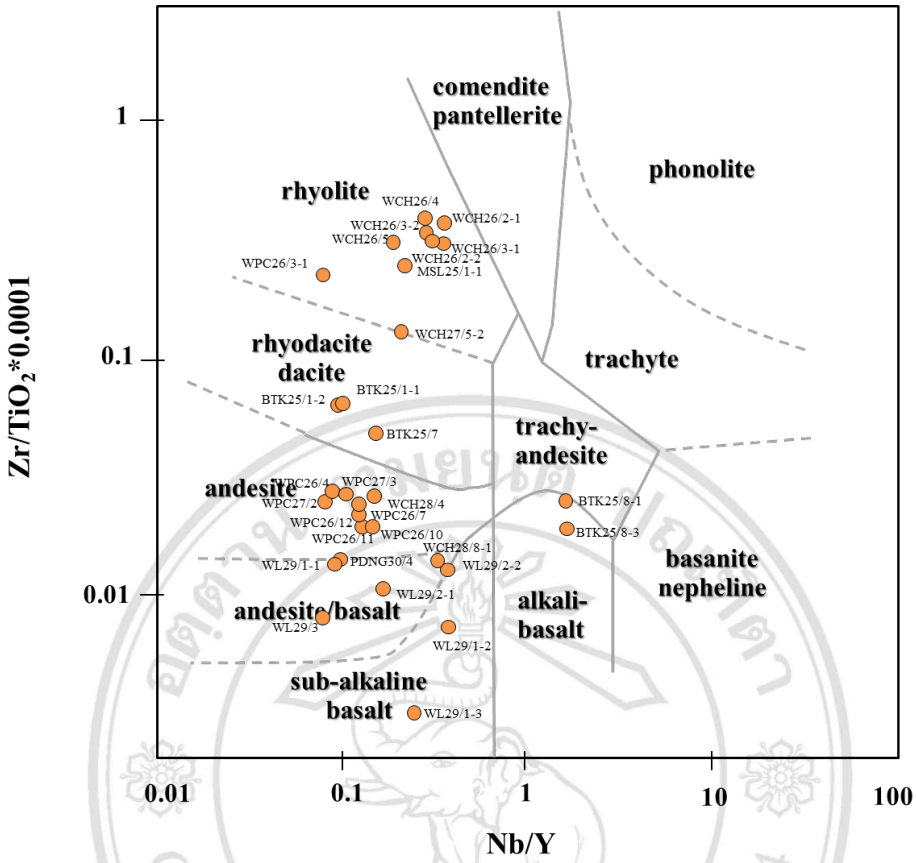

Figure 4.1 Plot of Zr/TiO_2 against Nb/Y for the studied, least-altered volcanic and associated rocks. Field boundaries for different magma types are after Winchester and Floyd (1977).

Two samples of the Group I rocks (sample number BTK25/1-2 and BTK25/7) were selected for REE analyses. They show a relatively flat REE patterns from Sm to Yb, with chondrite-normalized Sm/Yb [herein (Sm/Yb)cn] = 1.03-1.27, and slightly LREE enriched, with chondrite-normalized La/Sm [herein (La/Sm)cn] = 2.32-2.44 (Figure 4.2a). These REE patterns are typical of mildly calc-alkaline series.

4.3.2 Group II Rocks

The Group II rocks (sample number BTK 25/8-1 and BTK 25/8-3) were collected from the Mae Phrik area, and are basalt. They have Zr/TiO_2 against Nb/Y ratios in ranges of 0.0170-0.0208 and 2.4277-2.6089, respectively, corresponding alkaline series (Figure 4.1).

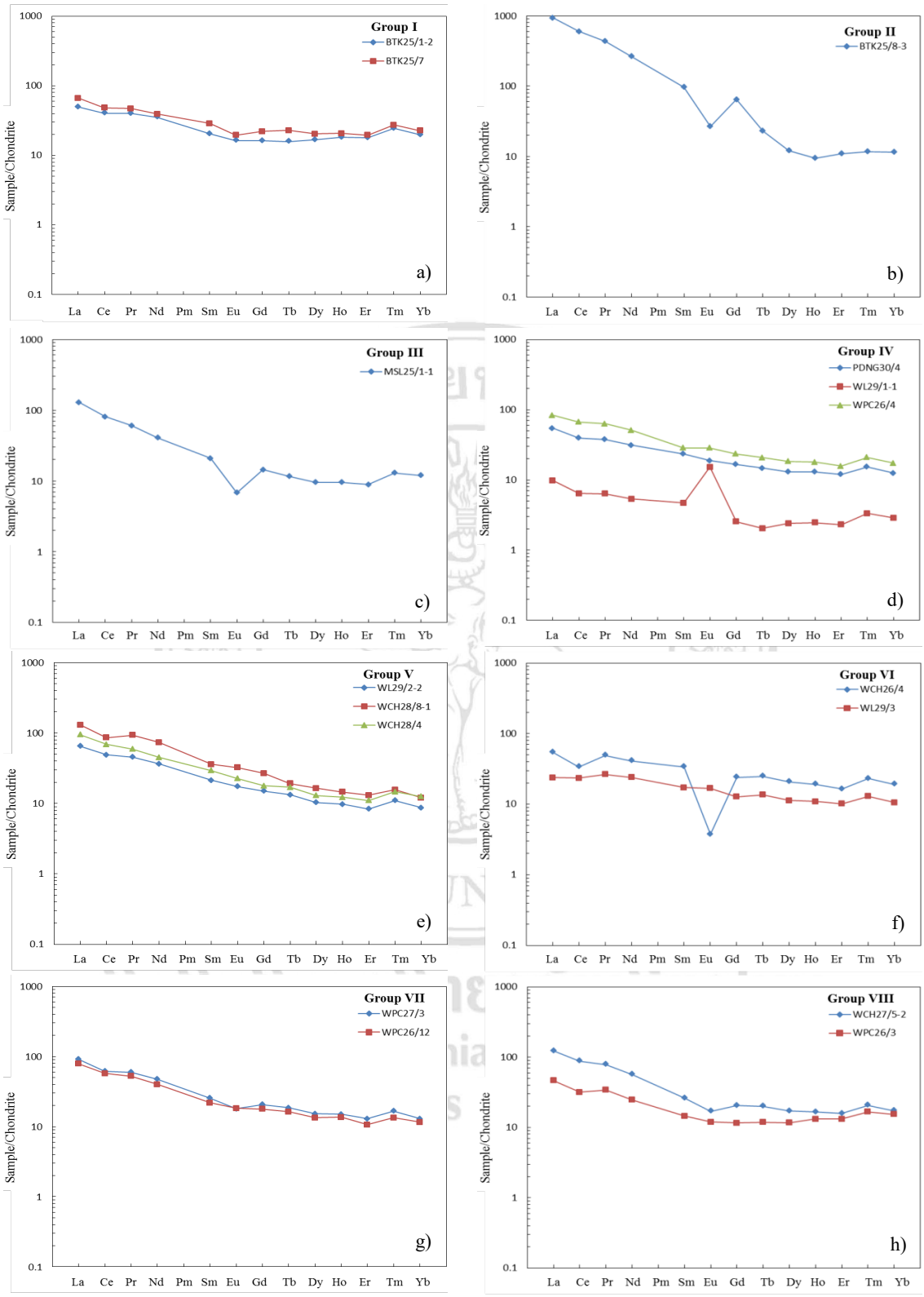

Figure 4.2 Chondrite-normalized patterns for the representatives of the studied volcanic and associated rocks. Chondrite-normalized values are those of Taylor and Gorton (1977).

One sample of the Group II rocks (sample number BTK25/8-3) was selected for REE analyses. It shows a relatively flat REE patterns from Sm to Yb, with chondrite-normalized Sm/Yb [herein (Sm/Yb)cn] = 8.40, and slightly LREE enriched, with chondrite-normalized La/Sm [herein (La/Sm)cn] = 9.67 (Figure 4.2b). This REE patterns are typical of alkaline series.

4.3.3 Group III Rocks

The Group III rock (sample number MSL25/1-1) was collected from the Mae Salaem area, and is rhyolite. It has Zr/TiO_2 against Nb/Y ratios in ranges of 0.2382 and 0.2214, respectively, corresponding subalkalic series (Figure 4.1).

The studied rock of the Group III rock shows a relatively flat REE patterns from Sm to Yb, with chondrite-normalized Sm/Yb [herein (Sm/Yb)cn] = 1.73, and slightly LREE enriched, with chondrite-normalized La/Sm [herein (La/Sm)cn] = 6.17 (Figure 4.2c). This REE patterns are typical of calc-alkaline series.

4.3.4 Group IV Rocks

The Group IV rocks (sample number PDNG30/4, WL29/1-1, WL29/1-2, WL29/1-3, WL29/2-1, and WPC26/4) were collected from the Pong Daeng, Wang Luek, and Wang Prachop areas. They comprise of basalt porphyry (PDNG30/4), cumulus gabbro (WL29/1-1, WL29/1-2, WL29/1-3, and WL29/2-1), and andesite porphyry (WPC26/4). They have Zr/TiO_2 against Nb/Y ratios in ranges of 0.0032-0.0276 and 0.0882-0.3732, respectively, corresponding subalkalic series (Figure 4.1).

Three samples of the Group IV rocks (sample number PDNG30/4, WL29/1-1, and WPC26/4) were selected for REE analyses. They show a relatively flat REE patterns from Sm to Yb, with chondrite-normalized Sm/Yb [herein (Sm/Yb)cn] = 1.63-1.88, and slightly LREE enriched, with chondrite-normalized La/Sm [herein (La/Sm)cn] = 2.10-2.91 (Figure 4.2d). These REE patterns are typical of mildly alkaline series. The REE patterns for the WL29/1-1 rocks have positive Eu anomaly, are controlled by cumulative plagioclase.

4.3.5 Group V Rocks

The Group V rocks (sample number WL29/2-2, WCH28/4, and WCH28/8-1) were collected from the Wang Luek and Wang Chao areas. They comprise of gabbro (WL29/2-2), andesite (WCH28/4), and basalt (WCH28/8). They have Zr/TiO_2 against Nb/Y ratios in ranges of 0.0131-0.0264 and 0.1497-0.3656, respectively, corresponding subalkalic series (Figure 4.1).

Three samples of the Group V rocks (WL29/2-2, WCH28/4, and WCH28/8-1) were selected for REE analyses. They show a relatively flat REE patterns from Sm to Yb, with chondrite-normalized Sm/Yb [herein (Sm/Yb)cn] = 2.33-2.99, and slightly LREE enriched, with chondrite-normalized La/Sm [herein (La/Sm)cn] = 3.05-3.60 (Figure 4.2e). These REE patterns are typical of alkaline series.

4.3.6 Group VI Rocks

The Group VI rocks (sample number WL29/3 and WCH26/4) were collected from the Wang Luek and WangChao areas. They comprise of gabbro (WL29/3) and rhyolite (WCH26/4). They have Zr/TiO_2 against Nb/Y ratios in ranges of 0.0079-0.3772 and 0.0776-0.3551, respectively, corresponding subalkalic series (Figure 4.1).

Two samples of the Group VI rocks (sample number WL29/3 and WCH 26/4) were selected for REE analyses. They show a relatively flat REE patterns from Sm to Yb, with chondrite-normalized Sm/Yb [herein (Sm/Yb)cn] = 1.63-1.76, and slightly LREE enriched, with chondrite-normalized La/Sm [herein (La/Sm)cn] = 1.39-1.61 (Figure 4.2f). These REE patterns are typical of tholeiitic series. The REE patterns for the WCH26/4 rocks have negative Eu anomaly suggested that this rhyolite do not have plagioclase crystallization.

4.3.7 Group VII Rocks

The Group VII rocks (sample number WPC26/7, WPC26/10, WPC26/11, WPC26/12, WPC27/2, and WPC27/3) were collected from the Wang Prachop area and are andesite porphyry. They have Zr/TiO_2 against Nb/Y ratios in ranges

of 0.0189-0.0267 and 0.0815-0.1458, respectively, corresponding subalkalic series (Figure 4.1).

Two samples of the Group VII rocks (sample number WPC26/12 and WPC27/3) were selected for REE analyses. They show a relatively flat REE patterns from Sm to Yb, with chondrite- normalized Sm/Yb [herein (Sm/Yb)cn] = 1.90-1.97, and slightly LREE enriched, with chondrite-normalized La/Sm [herein (La/Sm)cn] = 3.57-3.58 (Figure 4.2g). These REE patterns are typical of mildly calc-alkaline series.

4.3.8 Group VIII Rocks

The Group VIII rocks (sample number WPC26/3-1, WCH26/2-1, WCH26/2-2, WCH26/3-1, WCH26/3-2, WCH26/5, and WCH27/5-2) were collected from the Wang Prachop and Wang Chao areas and are rhyolite. They have Zr/TiO_2 against Nb/Y ratios in ranges of 0.1262-0.2999 and 0.0793-0.2100, respectively, corresponding subalkalic series (Figure 4.1).

Two samples of the Group VIII rocks (sample number WPC26/3-1 and WCH27/5-2) were selected for REE analyses. They show a relatively flat REE patterns from Sm to Yb, with chondrite-normalized Sm/Yb [herein (Sm/Yb)cn] = 0.95-1.50, and slightly LREE enriched, with chondrite-normalized La/Sm [herein (La/Sm)cn] = 3.20-4.69 (Figure 4.2h). These REE patterns are typical of mildly calc-alkaline series.

The negative Eu anomalies, even when plagioclase fractionation took place, may be because the magma was so oxidized that Eu^{+2} changed to Eu^{+3} and avoided it is presence in plagioclase crystals (Drake, 1975). A negative Ce anomaly has been widely used as a tracer for a subducted sediment component in convergent margins (Hole *et al.,* 1984; Neal and Taylor, 1989; Class and le Roex, 2008) like the Trans-Mexican Volcanic Belt (TMVB). This occurs because Ce is also controlled by its oxidation and reduction chemistry, so the oxidation of the soluble Ce^{+3} to the insoluble Ce^{+4} produces the negative Ce anomaly in pelagic sediments. If this is true, the subducted sediments

could react with surrounding mantle minerals to imprint its Ce anomaly (Class and le Roex, 2008).

In term of N-MORB normalized multi-element patterns, the studied rocks show negative niobium and tantalum anomalies (Figure 4.3). Nb and Ta anomalies are characteristic of the magmas associated with subduction zones. They are more primitive and are associated with the presence in the mantle of a phase which is stable under the P, T, and H_2O conditions generated by the geodynamic context (Briqueu *et al.*, 1984). N-MORB normalized multi-element patterns for the Group I, Group II, Group V, Group VI, Group VII, and Group VIII rocks show negative phosphorus and titanium anomalies. The multi-element pattern shows negative anomalies in P and Ti in relation to their more evolved composition (Demant *et al.*, 2007).

The variation diagrams for least-mobile elements of the volcanic and associated rocks, using Zr as a fractionation parameter are shown in Figure 4.4 for major oxides and Figure 4.5 for trace elements.

The binary ratios and patterns of plotting in variation diagrams for eight groups supported that they are not comagmatic.

4.4 Alteration Index

In the Molar K/Al vs. molar (K+Na+2Ca)/Al (Madeisky, 1996; Booden *et al.*, 2010) diagram that shoes the alteration minerals kaolinite, illite and adularia plot on a line of slope 1. Unaltered igneous rocks typically have molar (K+Na+2Ca)/Al values >1. Potassium metasomatism leads to decreasing molar (K+Na+2Ca)/Al and increasing molar K/Al values, which is partly observed for the studied rocks particularly for Group I and Group II. Most of the studied rocks have molar (K+Na+2Ca)/Al >1or close to (0.9) and considered to be the least altered rocks (Figure 4.6). So the studied rocks can use for identification of rock types, determining magma characteristics and interpretation of tectonic setting of formation.

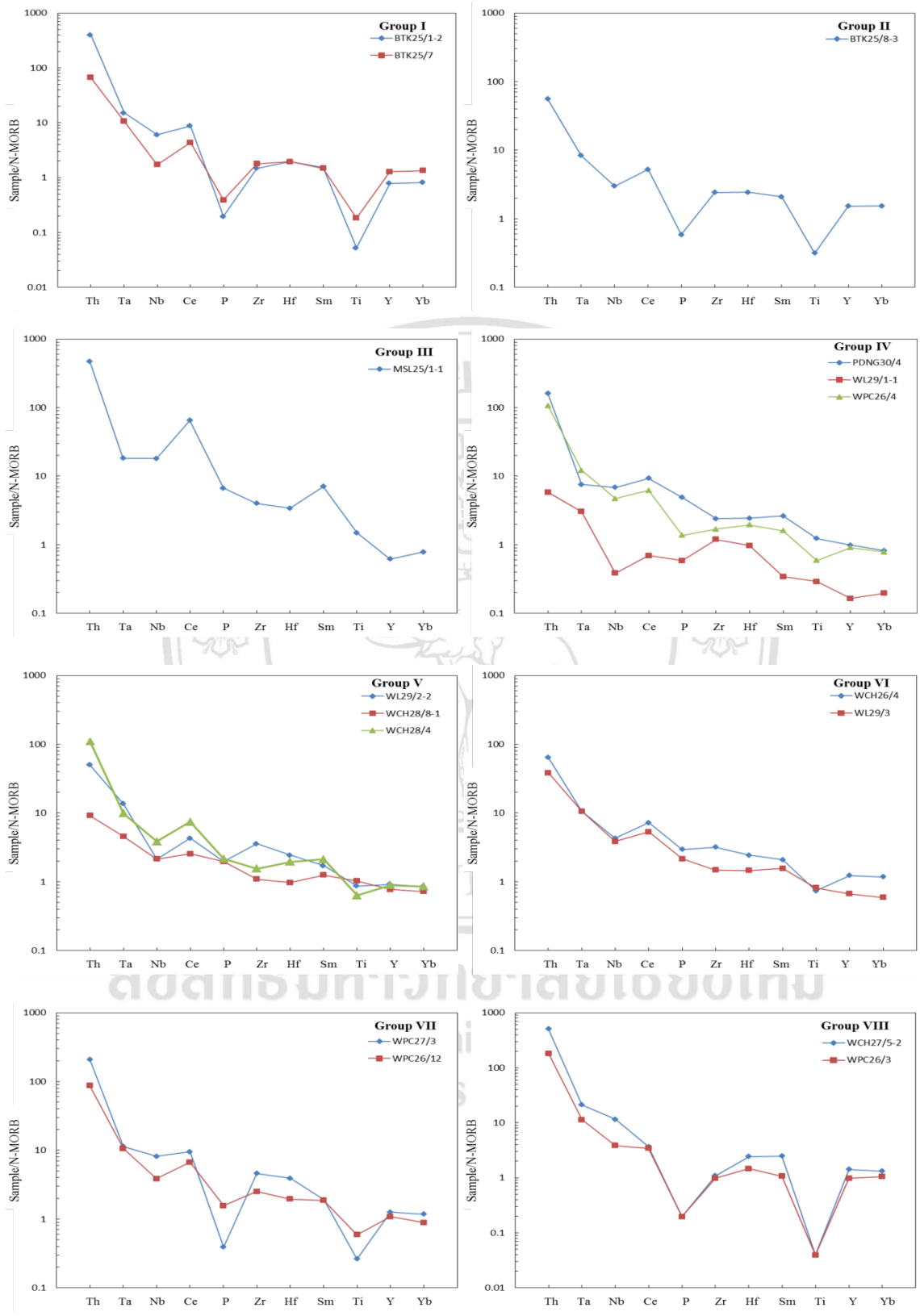

Figure 4.3 N-MORB normalized multi-element patterns for the representatives of volcanic and associated rocks. N-MORM normalized values are those of Sun and McDonough (1989).

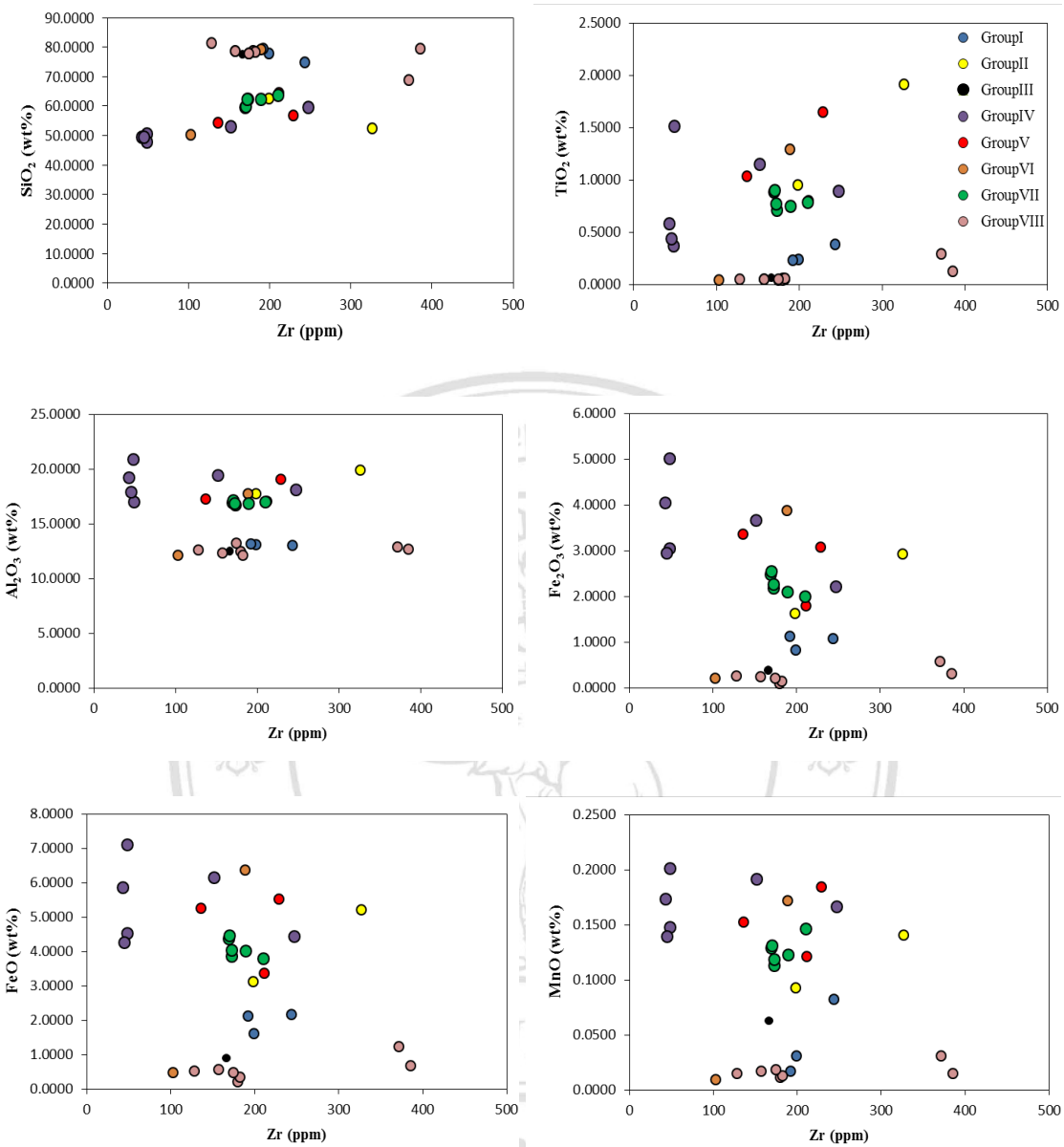

Figure 4.4 Zirconia variation diagrams for SiO_2, TiO_2, Al_2O_3, Fe_2O_3, FeO, MnO, MgO and CaO for the studied, least-altered volcanic and associated rocks. Zr is expressed as ppm, whereas major oxides as wt%.

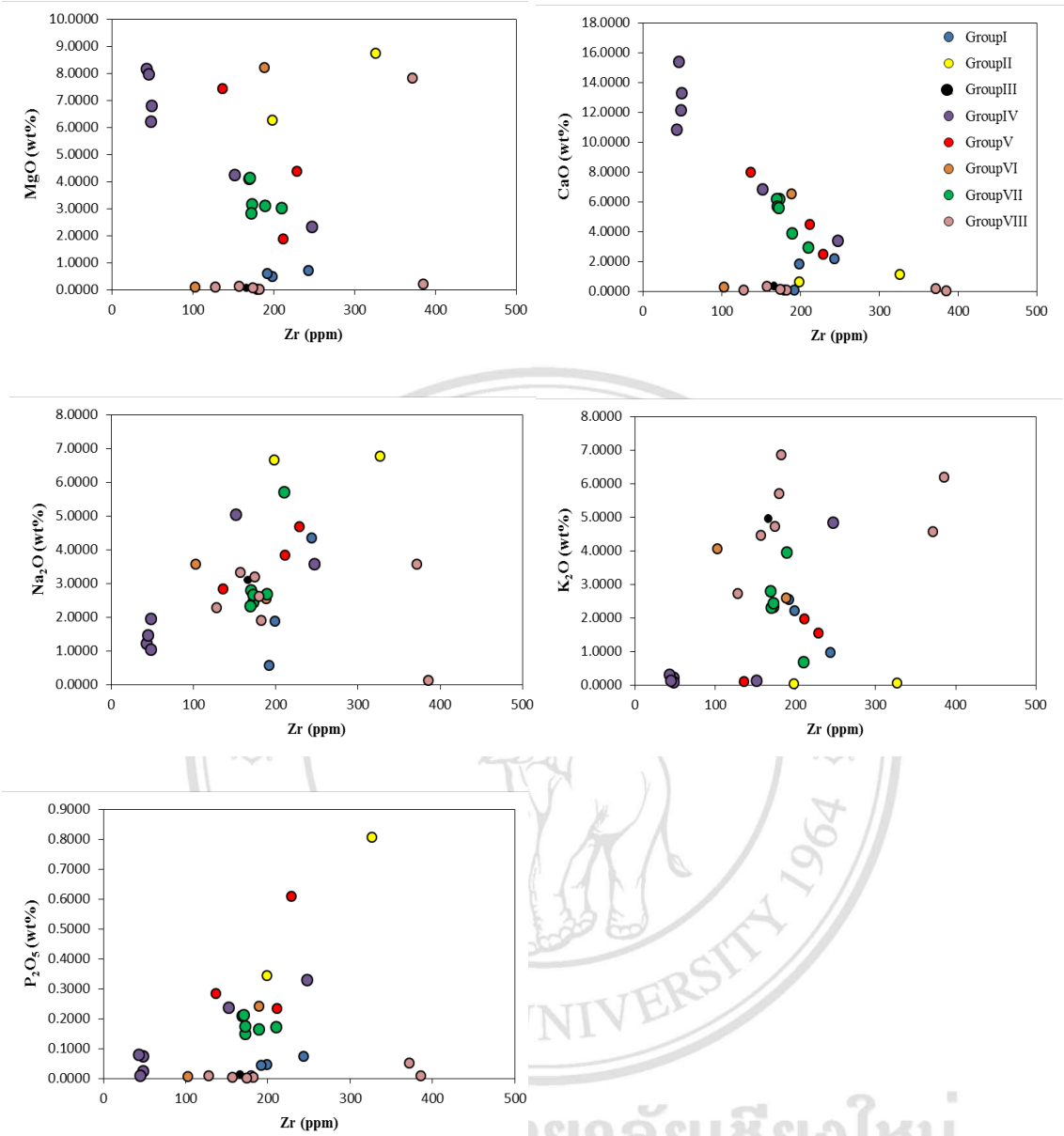

Figure 4.4 continued

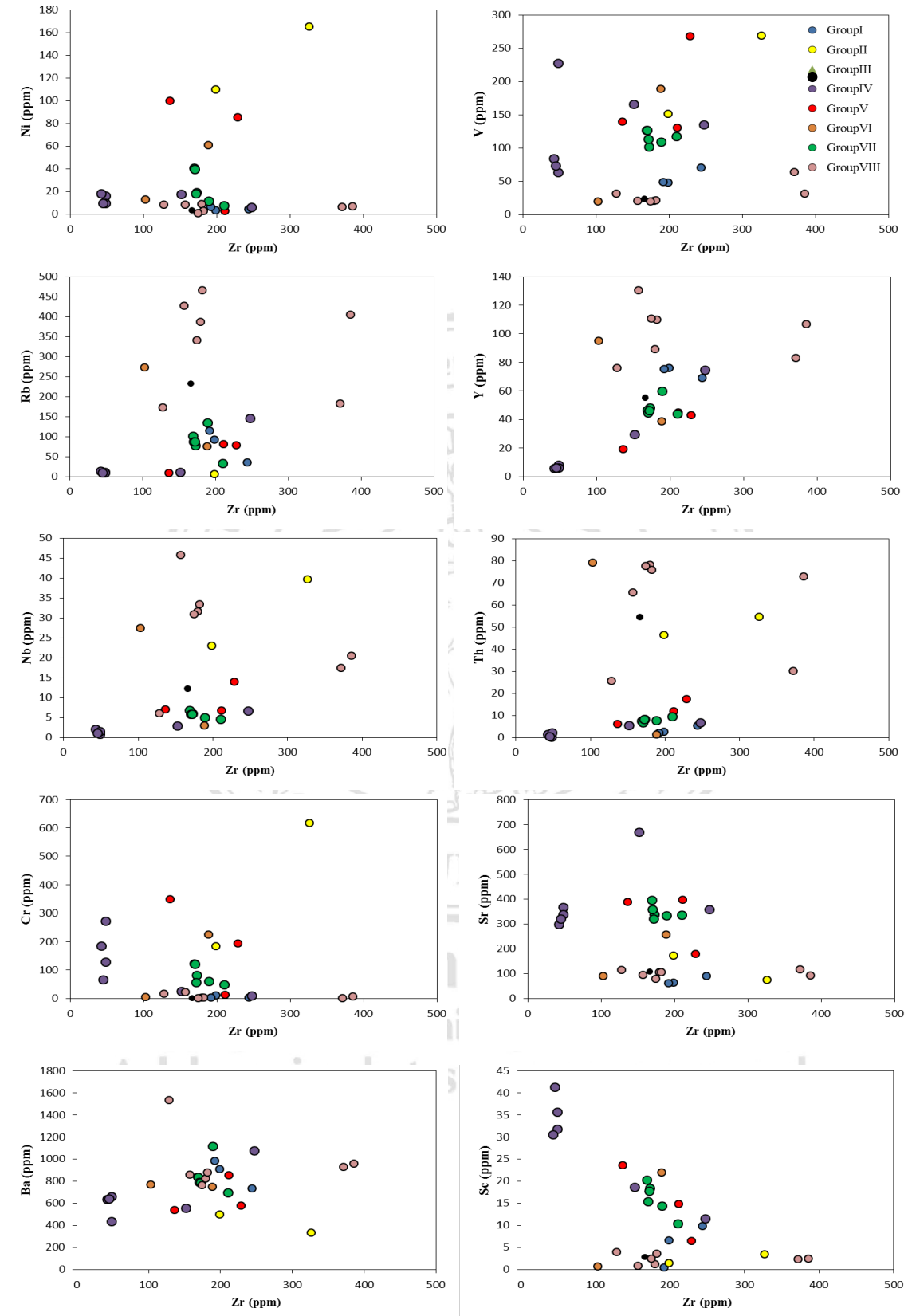

Figure 4.5 Zirconia variation diagrams for Ni, V, Rb, Y, Nb, Th, Cr, Sr, Ba and Sc for the studied, least-altered volcanic and associated rocks. The trace elements are in ppm.

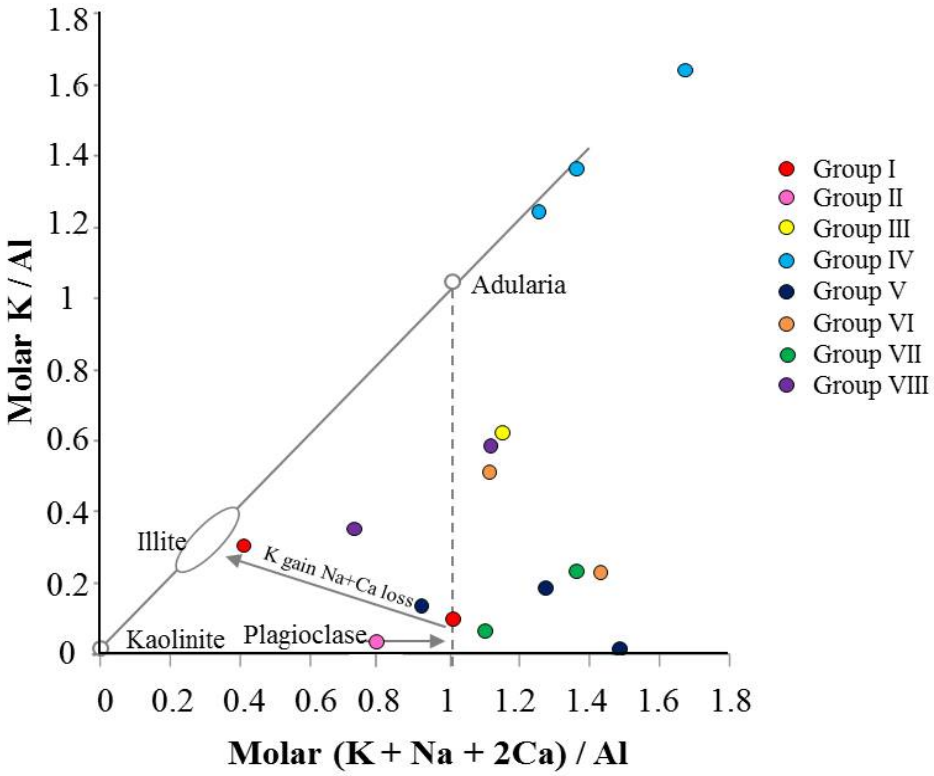

Figure 4.6 Molar K/Al vs. molar (K+Na+2Ca)/Al (Madeisky, 1996; Booden *et al*., 2010). In this diagram, the alteration minerals kaolinite, illite and adularia plot on a line of slope 1. Unaltered igneous rocks typically have molar (K+Na+2Ca)/Al values >1. Potassium metasomatism leads to decreasing molar (K+Na+2Ca)/Al and increasing molar K/Al values.

4.5 Tectonic Setting of Eruption

The chemical compositions of the studied rocks will provide for interpretation of tectonic setting by using discrimination diagram and correlation with modern magma suites. Many researchers analyzed and created the tectonic discrimination diagrams for interpretation of tectonic setting of igneous rocks. The tectonic discrimination diagrams of felsic and mafic rocks present in this chapter except the diagram of ultramafic and cumulative rocks. Carefully plot the geochemistry data of felsic and mafic rocks in their own diagrams.

4.5.1 Tectonic Discrimination Diagrams

Discrimination diagrams (Rollison, 1993) is geochemical variation diagrams on which magmas produced in different tectonic settings may be distinguished from one another on the basis of their chemistry. The elemental concentrations were calculated discrimination functions based upon the elemental concentrations, boundaries are drawn between the different groups of samples. The diagrams used to discriminate tectonic environments of the studied felsic volcanic rocks include Y-Nb (Figure 4.7a) and (Y+Nb) vs. Rb (Figure 4.7b).

Both of studied rhyolite and rhyodacite are presenteded in the within plate granite field except WPC26/3-1 which is emerge to be the orogeny granite field in Y-Nb diagram. May be support with field occurrence that occurred in chill margin of granite intrusive (Singtuen and Phajuy, 2017).

The diagrams used to discriminate tectonic environments of the studied mafic rocks include Ti/Y-Nb/Y (Figure 4.8), V-Ti (Figure 4.9), Zr/Y-Ti/Y (Figure 4.10), Zr/Y-Zr (Figure 4.11), Cr-Y (Figure 4.12), Nb/Y-Zr/P_2O_5 (Figure 4.13), and TiO_2-Y/Nb (Figure 4.14), and Ti-Zr (Figure 4.15) bivariate plots and Zr-Nb-Y (Figure 4.16), Zr-Ti-Y (Figure 4.17), Th-Hf-Ta (Figure 4.18) and La-Y-Nb (Figure 4.19) ternary plots.

The Group II rocks are largely presented in the fields of volcanic arc with subordinate within-plate basalt, mid-oceanic ridge basalt and calc-alkalic basalt. The volcanic arc is presented in Ti-Zr (Figure 4.15a) and Th-Hf-Ta (Figure 4.18) diagrams. The within-plate basalt is presented in Ti-Zr (Figure 4.15a) diagram. Whereas the mid- oceanic ridge basalt is presented in V-Ti (Figure 4.9) diagram. These rocks, however, appear to be calc-alkalic basalt is presented in La-Y-Nb (Figure 4.19) diagrams.

The Group IV rocks mostly emerge to be the fields of volcanic arc and within-plate basalt, with subordinate mid-oceanic ridge basalt, plate margin, continental tholeiitic basalt, ocean tholeittic basalt and calc-alkalic basalt. The volcanic arc is presented in Ti/Y-Nb/Y (Figure 4.8), V-Ti (Figure 4.9), Ti-Zr

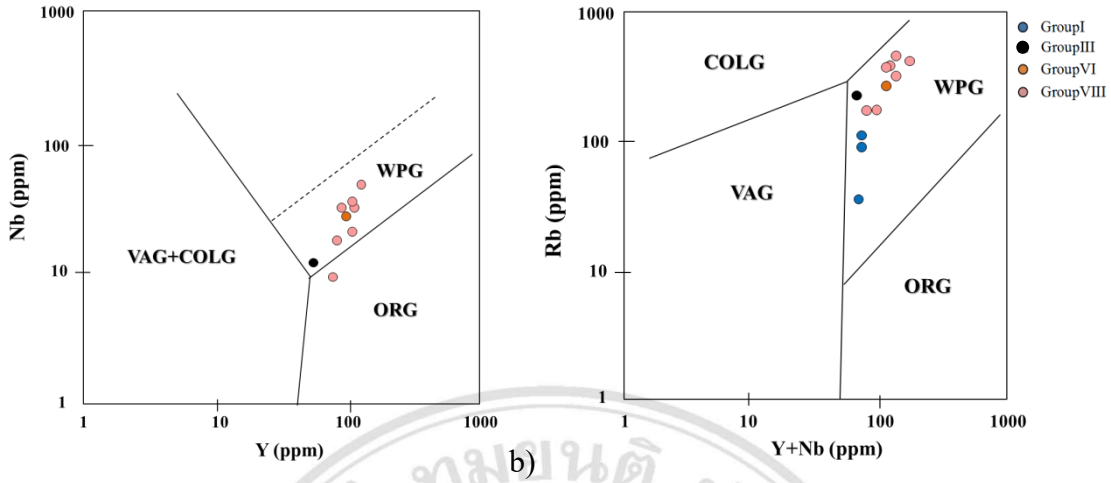

Figure 4.7 a) Y vs. Nb and b) (Y+Nb) vs. Rb plots for the studied felsic volcanic rocks (Pearce et al., 1984) VAG = volcanic arc granite, COLG = collision orogeny granite, WPG = within plate granite, and ORG = orogeny granite

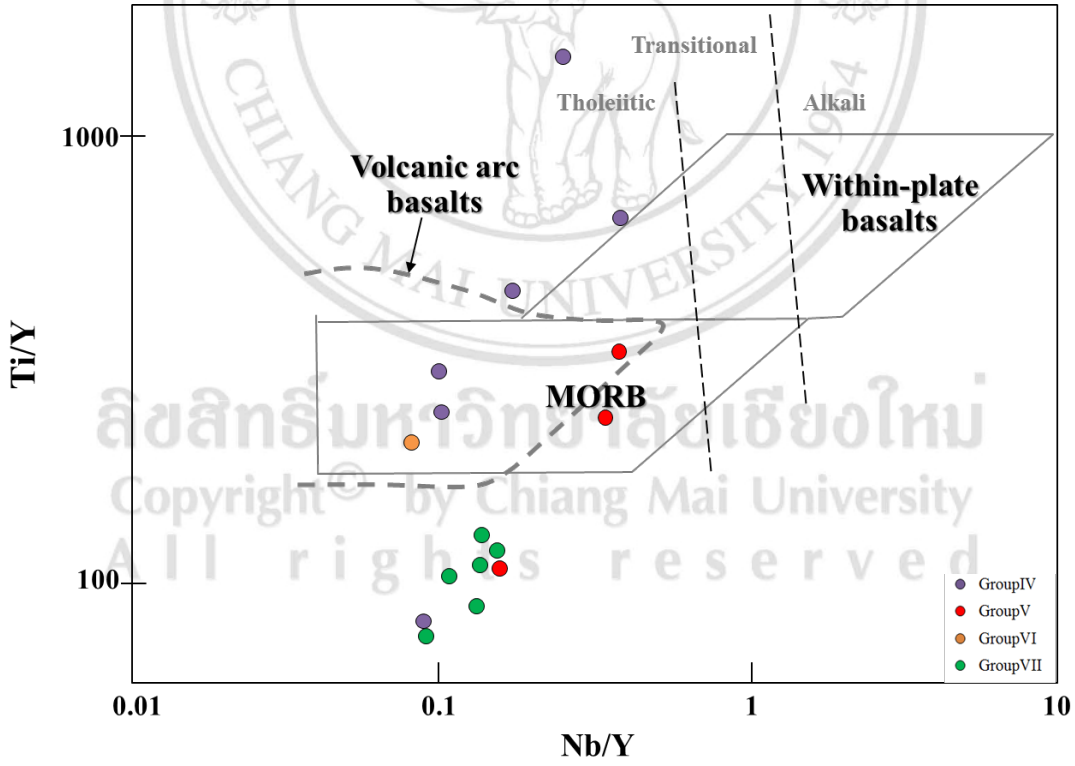

Figure 4.8 Ti/Y-Nb/Y discrimination diagram (after Pearce, 1982) for the studied, least-altered mafic volcanic and associated rocks. MORB = mid-oceanic ridge basalt.

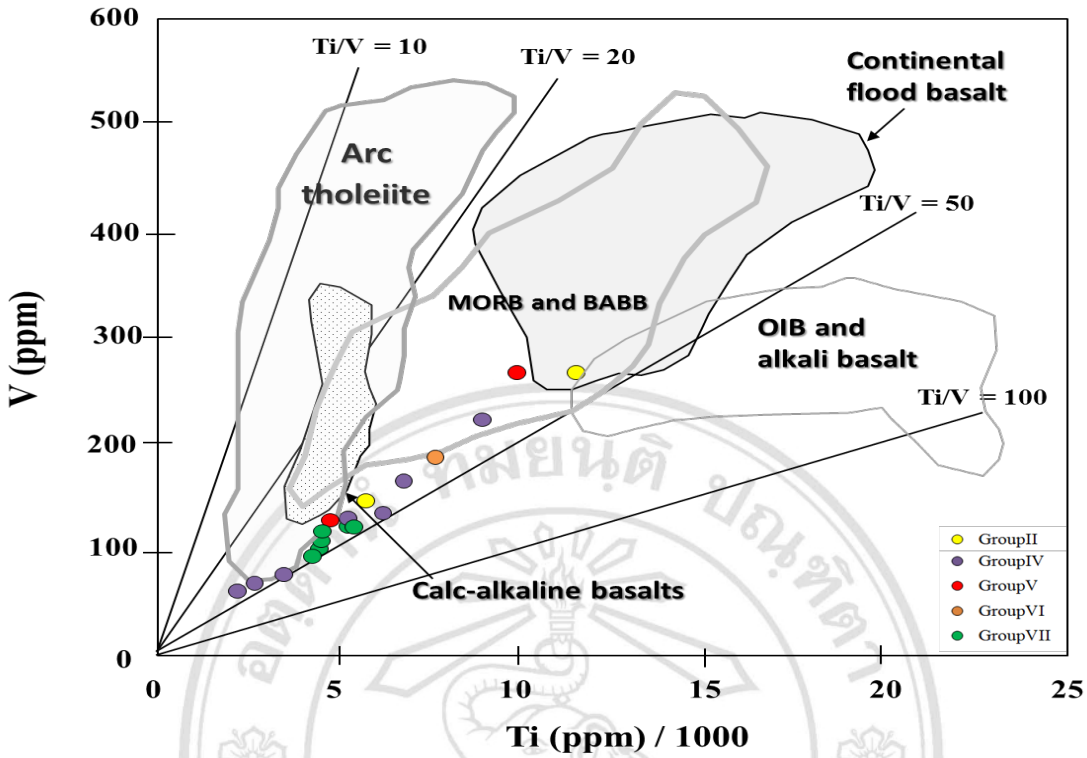

Figure 4.9 Ti-V tectonic discrimination diagram (after Shervais, 1982) for the studied, least-altered mafic volcanic and associated rocks.

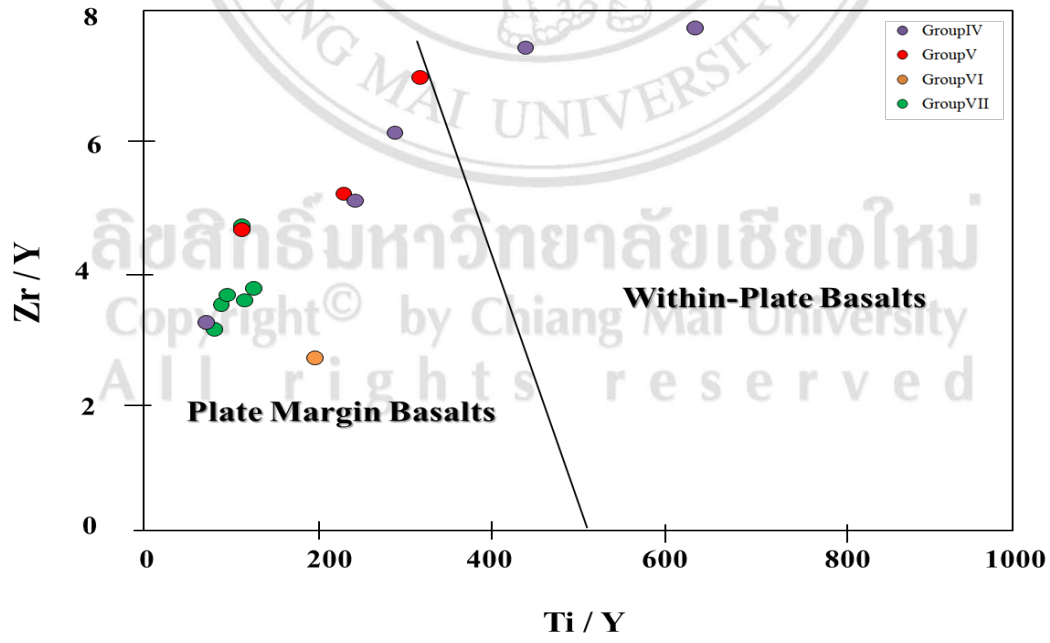

Figure 4.10 Zr/Y-Ti/Y discrimination diagram between plate-margin basalt and within-plate basalt (after Pearce and Gale, 1977) for the studied, least-altered mafic volcanic and associated rocks.

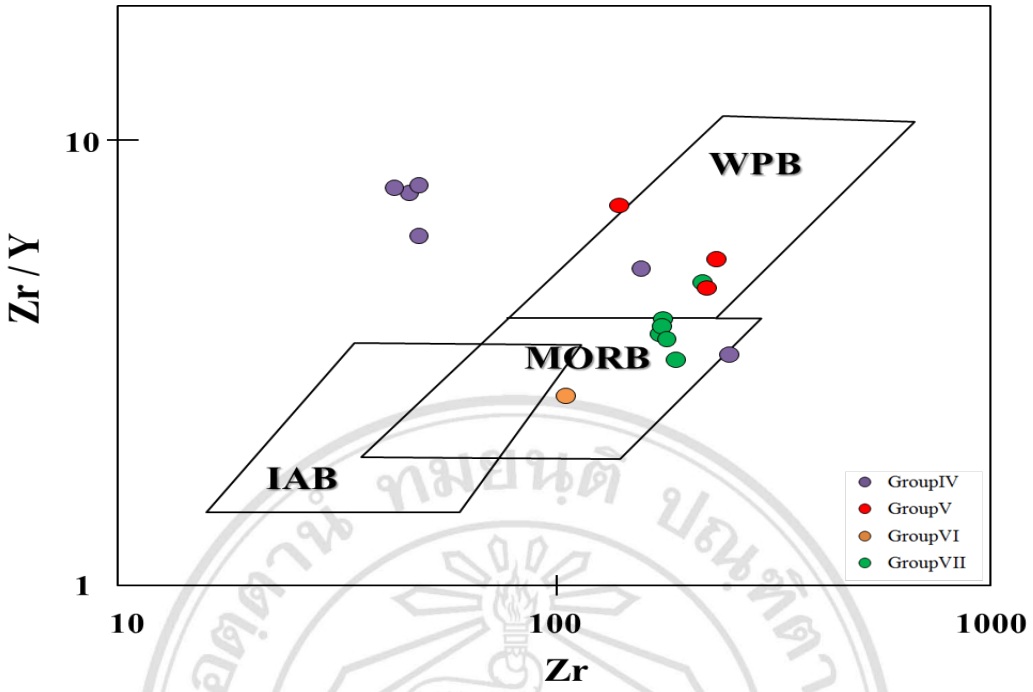

Figure 4.11 Zr/Y-Zr discrimination diagram (after Pearce and Norry, 1979) for the studied, least-altered mafic volcanic and associated rocks. The fields are as follow: IAT = island-arc tholeiite, MORB = mid-oceanic ridge basalt, WPB = within-plate basalt.

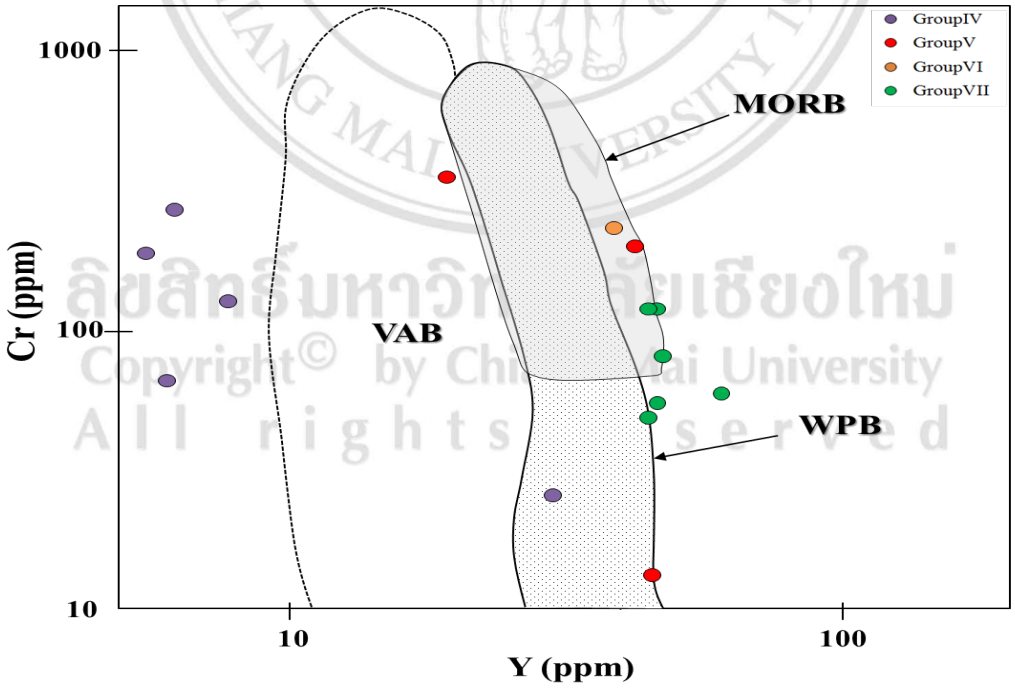

Figure 4.12 Cr-Y discrimination diagram (after Pearce, 1982) for the studied, least-altered mafic volcanic and associated rocks. The fields are as follow: VAB = volcanic-arc basalt, MORB = mid-oceanic ridge basalt, WPB = within-plate basalt.

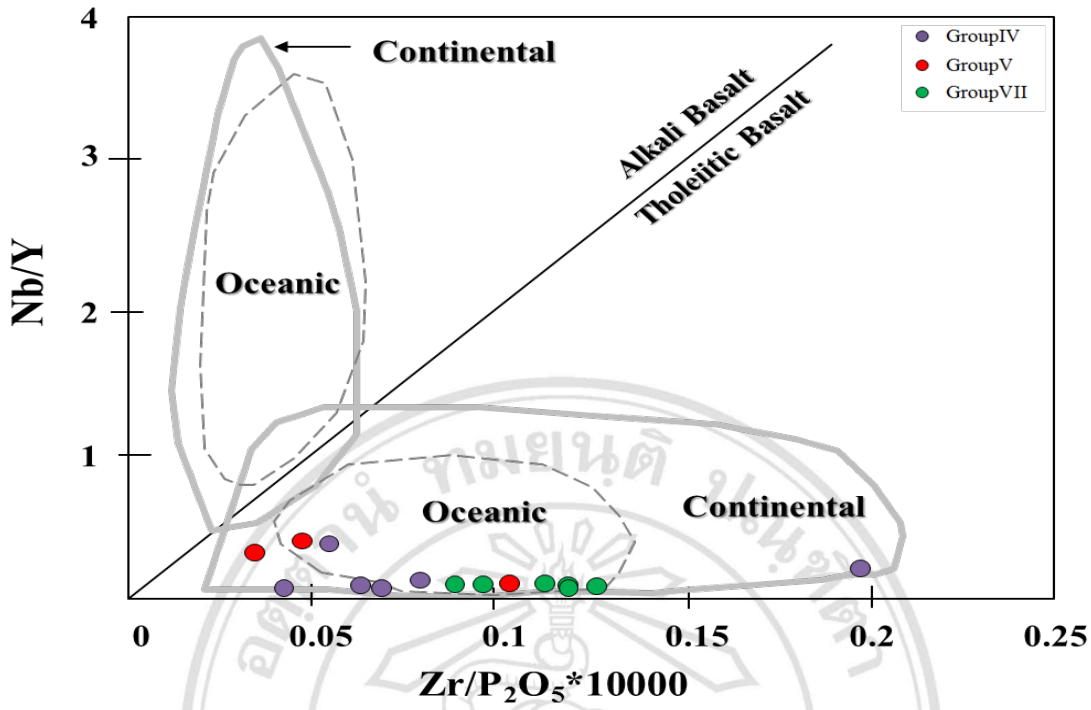

Figure 4.13 Nb/Y-Zr/P_2O_5 discrimination diagram (adapted from Floyd and Winchester, 1975) for the studied, least-altered mafic volcanic and associated rocks. Showing fields of continental and oceanic alkali basalts and tholeiitic basalts.

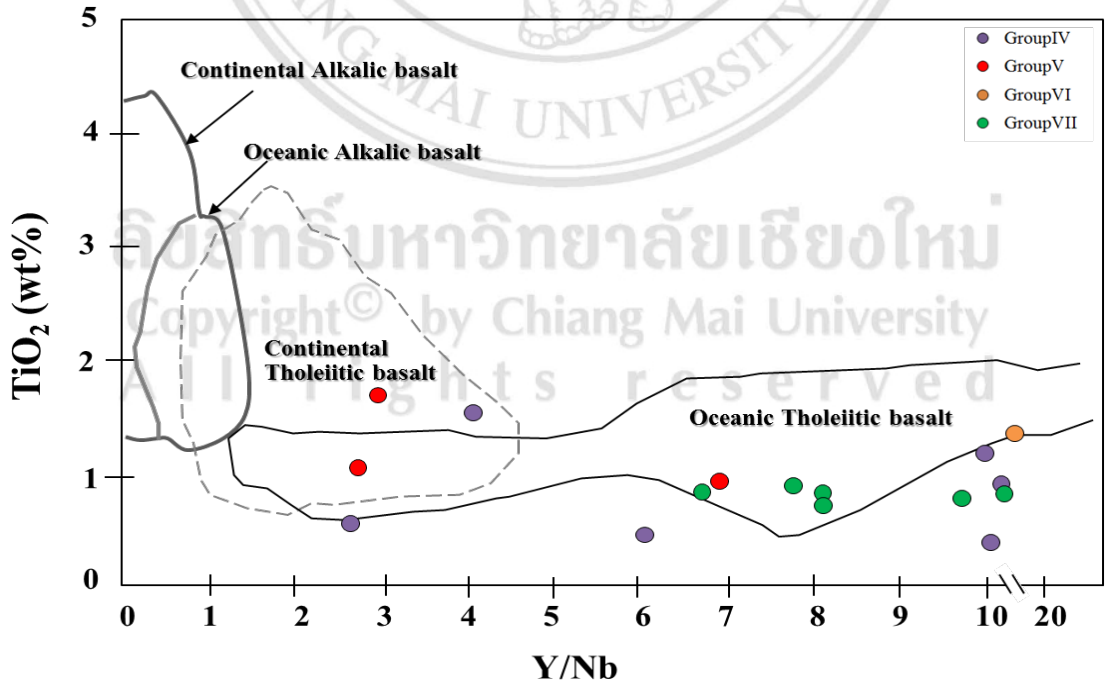

Figure 4.14 TiO_2-Y/Nb discrimination diagram (from Floyd and Winchester, 1975) for the studied, least-altered mafic volcanic and associated rocks.

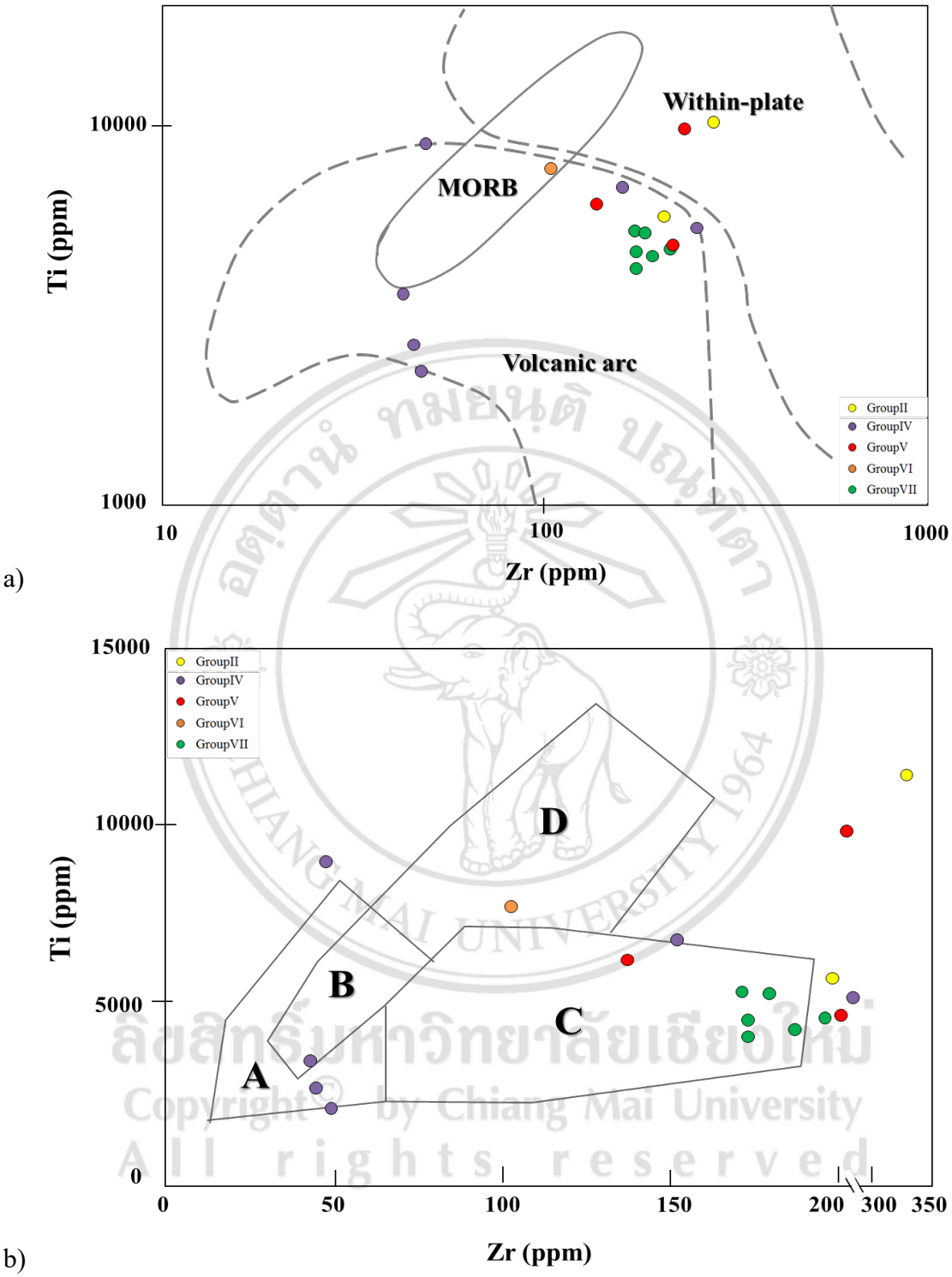

Figure 4.15 Ti-Zr discrimination diagram for the studied, least-altered mafic volcanic and associated rocks, (a) after Pearce (1982) and (b) after Pearce and Cann (1973); the fields are as follows: MORB = mid-oceanic ridge basalt, A = island-arc tholeiites, B = mid-oceanic ridge basalt, calc-alkali basalts and island-arc tholeiites, C = calc-alkali basalts and D = mid-oceanic ridge basalt.

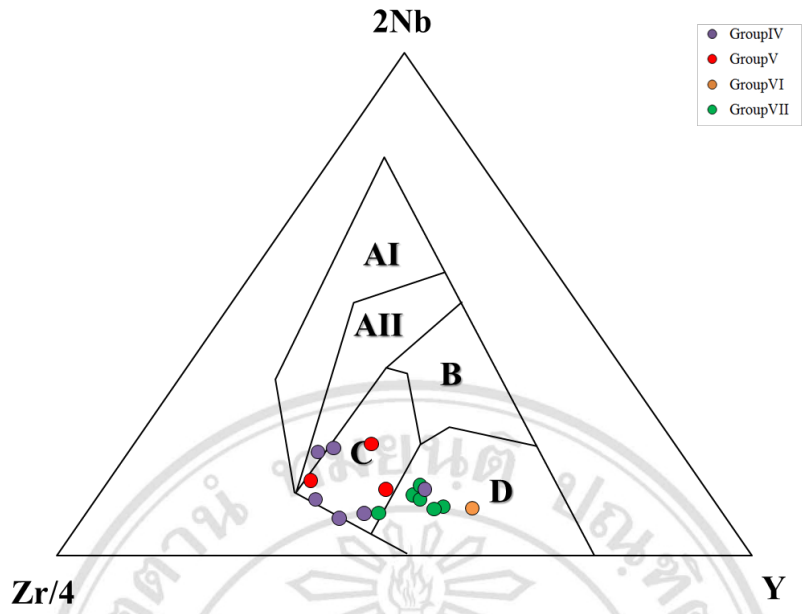

Figure 4.16 The Zr-Nb-Y discrimination diagram for the studied, least-altered mafic volcanic and associated rocks (after Meschede, 1986). The fields are defined as follows; AI = within-plate alkali basalts, AII = within-plate alkali basalts and within-plate tholeiites, B = enriched-mid oceanic ridge basalts, C = within-plate tholeiites and volcanic-arc basalts and D = normal-mid oceanic ridge basalts and volcanic-arc basalts.

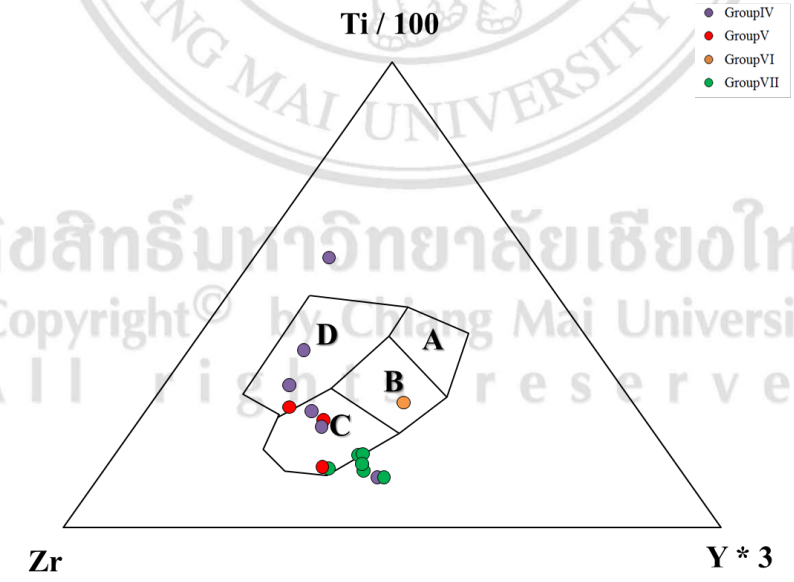

Figure 4.17 The Zr-Ti-Y discrimination diagram for the studied, least-altered mafic volcanic and associated rocks (after Pearce and Cann, 1973). The fields are as follows: A = island-arc tholeiite, C = calc-alkali basalt, D = within-plate basalt and B = MORB, island-arc tholeiite and calc-alkali basalt.

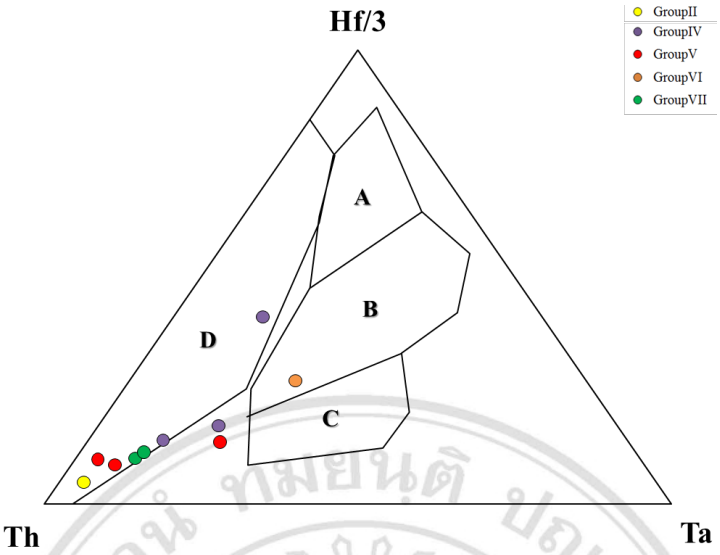

Figure 4.18 The Th-Hf-Ta discrimination diagram (after Wood, 1980) for the studied, least-altered mafic volcanic and associated rocks. The fields are: A = normal mid-oceanic ridge basalts, B = enriched-mid oceanic ridge basalts and within-plate tholeiite, C = within-plate alkali basalt and D = volcanic-arc basalt. Island-arc tholeiite is in the field D where Hf/Th>3.0 and calc-alkalic basalt where Hf/Th<3.0.

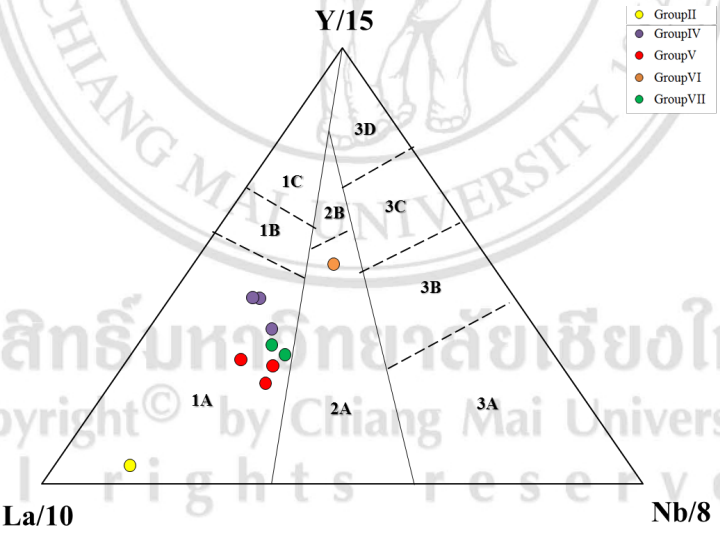

Figure 4.19 The La-Y-Nb discrimination diagram (after Cabanis and Lecolle, 1989) for the studied, least-altered mafic volcanic and associated rocks. Field1 contains volcanic-arc basalt, field2 continental basalt, and field3 oceanic basalt. The subdivisions of the fields are as follows: 1A = calc-alkali basalt, 1C = volcanic-arc tholeiite, 1B = calc-alkali basalt and volcanic are tholeiite, 2A = continental basalt, 2B = back-arc basin, 3A = alkali basalt from intercontinental rift, 3B+3C = enriched-mid oceanic ridge basalts (3B enriched, 3C weakly enriched), and 3D = normal-mid oceanic ridge basalts.

(Figure 4.15), Zr-Nb-Y (Figure 4.16), and Th-Hf-Ta (Figure 4.18) diagram. These rocks, however, appear to be within-plate basalt is located in Zr/Y-Ti/Y (Figure 4.10), Zr/Y-Zr (Figure 4.11), Cr-Y (Figure 4.12), Zr-Nb-Y (Figure 4.16), and Zr-Ti-Y (Figure 4.17) diagrams. Whereas the mid-oceanic ridge basalt is presented in V-Ti (Figure 4.9) and Zr/Y-Zr (Figure 4.11) diagrams. These studied rock samples might have been formed in plate margin environment, as evidenced by their positions in the plot of Zr/Y-Ti/Y (Figure 4.10) diagram. In addition, the studied rock samples could well be continental and oceanic tholeiitic basalt as suggested by their positions in the Nb/Y-Zr/P_2O_5 (Figure 4.13) and TiO_2-Y/Nb (Figure 4.14) diagrams. While the calc-alkalic basalt is presented in Zr-Ti-Y (Figure 4.17) and La-Y-Nb (Figure 4.19) diagrams. The cumulative rocks inappropriately plot in all of diagrams so these rocks cannot interpret tectonic setting by discrimination diagrams.

The Group V rocks are largely presented in the fields of volcanic arc and within-plate basalt, with subordinate mid-oceanic ridge basalt, plate margin, continental tholeiitic basalt, ocean tholeittic basalt and calc-alkalic basalt. The volcanic arc is shown in Ti/Y-Nb/Y (Figure 4.8), V-Ti (Figure 4.9), Cr-Y (Figure 4.12), Ti-Zr (Figure 4.15), Zr-Nb-Y (Figure 4.16), and Th-Hf-Ta (Figure 4.18) diagram. These rocks, however, appear to be within-plate basalt is located in Zr/Y-Zr (Figure 4.11), Cr-Y (Figure 4.12), Ti-Zr (Figure 4.15a), Zr-Nb-Y (Figure 4.16), and Zr-Ti-Y (Figure 4.17) diagrams. On the other hand, the mid-oceanic ridge basalt is presented in Ti/Y-Nb/Y (Figure 4.8), V-Ti (Figure 4.9) and Cr-Y (Figure 4.12) diagrams. These studied rock samples might have been formed in plate margin environment, as evidenced by their positions in the plot of Zr/Y-Ti/Y (Figure 4.10) diagram. In addition, the studied rock samples could well be continental and oceanic tholeiitic basalt as suggested by their positions in the Nb/Y-Zr/P_2O_5 (Figure 4.13) and TiO_2-Y/Nb (Figure 4.14) diagrams. Whereas these rocks is shown in calc-alkalic basalt field, as evidenced in the plot of Ti-Zr (Figure 4.15b), Zr-Ti-Y (Figure 4.17) and La-Y-Nb (Figure 4.19) diagrams.

The Group VI rocks are largely distributed around the boundary of mid-oceanic ridge basalt and volcanic arc, with subordinate within-plate basalt, plate

margin, ocean tholeittic basalt, calc-alkalic basalt, and continental basalt. The mid-oceanic ridge basalt is presented in V-Ti (Figure 4.9), Zr/Y-Zr (Figure 4.11), Cr-Y (Figure 4.12), Ti-Zr (Figure 4.15), Zr-Nb-Y (Figure 4.16), Zr-Ti-Y (Figure 4.17), and Th-Hf-Ta (Figure 4.18) diagrams. While the volcanic arc is emerged in Ti/Y-Nb/Y (Figure 4.8), Ti-Zr (Figure 4.15), and Zr-Ti-Y (Figure 4.17) diagrams. These rocks, however, appear to be within-plate basalt is located in Th-Hf-Ta (Figure 4.18) diagram. These studied rock samples might have been formed in plate margin environment, as evidenced by their positions in the plot of Zr/Y-Ti/Y (Figure 4.10) diagram. On the other hand, the studied rock samples could well be oceanic tholeiitic basalt as suggested by their positions in the TiO_2-Y/Nb (Figure 4.14) diagram. While these rocks is shown in calc-alkalic basalt field, as evidenced in the plot of Zr-Ti-Y (Figure 4.17). In addition, the studied rock samples could well be continental basalt as suggested by their positions in the La-Y-Nb (Figure 4.19) diagram.

The Group VII rocks are largely shown in the fields of volcanic arc and mid-oceanic ridge basalt and within-plate basalt, with subordinate plate margin, ocean tholeittic basalt, and calc-alkalic basalt. The volcanic arc is emerged in V-Ti (Figure 4.9), Ti-Zr (Figure 4.15), Zr-Nb-Y (Figure 4.16), and Th-Hf-Ta (Figure 4.18) diagrams. Whereas mid-oceanic ridge basalt is presenteded in Zr/Y-Zr (Figure 4.11), Cr-Y (Figure 4.12), and Zr-Nb-Y (Figure 4.16) diagrams. These rocks, however, appear to be within-plate basalt is located in Zr/Y-Zr (Figure 4.11), Cr-Y (Figure 4.12), and Zr-Nb-Y (Figure 4.16) diagrams. These studied rock samples might have been formed in plate margin environment, as evidenced by their positions in the plot of Zr/Y-Ti/Y (Figure 4.10) diagram. In addition, the studied rock samples could well be oceanic tholeiitic basalt as suggested by their positions in the Nb/Y-Zr/P_2O_5 (Figure 4.13) and TiO_2-Y/Nb (Figure 4.14) diagrams. While these rocks is shown in calc-alkalic basalt field, as evidenced in the plot of Zr-Ti-Y (Figure 4.17) and La-Y-Nb (Figure 4.19) diagrams.

4.5.2 Modern Analogue

Although many tectonic discrimination diagrams have been appeared in literature, a number of researchers (e.g. Holm, 1982; Prestvik, 1982; Duncan,

1987; and Myers and Breitkopf, 1989) demonstrated that these diagrams may often fail to unequivocally classify tectonic setting of formation. This is also true for some magmatic groups presented in this study, i.e. the diagrams yield inconsistent results (see Section 4.5.1). Consequently, geochemical comparisons, extensive searches for modern analogue have been made in terms of chondrite-normalized REE and N-MORB normalized multi-element patterns. The modern analogues have been carried out to classify the tectonic settings of formation and for particular magmatic groups are given below.

The Group I rocks are closely similar in chemical composition to Miocene intra-plate A2-type rhyolites from Jabal Shama, Saudi Arabia (Surour *et al.,* 2016) (Figure 4.20). Miocene rhyolites (19.2 ± 0.9 Ma) at the Jabal Shama in western Saudi Arabia have been formed within a plate on the rifting stage in western of Arabia shield. They mostly consist of tuffaceous varieties with distinct flow banding, and pea-sized spherulites, obsidian and perlitized rhyolite tuffs. Although they have the geochemical signature of A2-type rhyolites, these silicic rocks are not typically alkaline but alkali-calcic to calc-alkaline. They developed in a within-plate regime and possibly derived from a recycled mafic subducted slab in depleted sub-continental mantle beneath the western Arabian plate.

The representatives of the Group II rocks are chemically comparable with the Miocene basaltic dike from Miocene magmatism in the Yaguila-Sharang district, Tibet (Zhao *et al.,* 2016) (Figure 4.21). In addition, the Group III rocks have very similar in chemical composition to Miocene rhyolite porphyry from Miocene magmatism at Yaguila, Tibet (Zhao *et al.,* 2016) (Figure 4.21). The Paleocene-Eocene ore deposits in the Gangdese Metallogenic Belt, Tibet, which have been formed as a post-collision between India and the Eurasia plates in the northern Himalayan orogeny. Geochemical signatures and Nd-Hf isotopic compositions indicate that the Yaguila Cretaceous rhyolitic rocks were formed by the melting of ancient continental crust, whereas the Paleocene causative granite porphyry may have resulted from the interaction between mantle-derived and crustal-derived materials when continental collision was initiated. The post-ore Miocene granodiorite porphyry has a similar geochemical signature to the

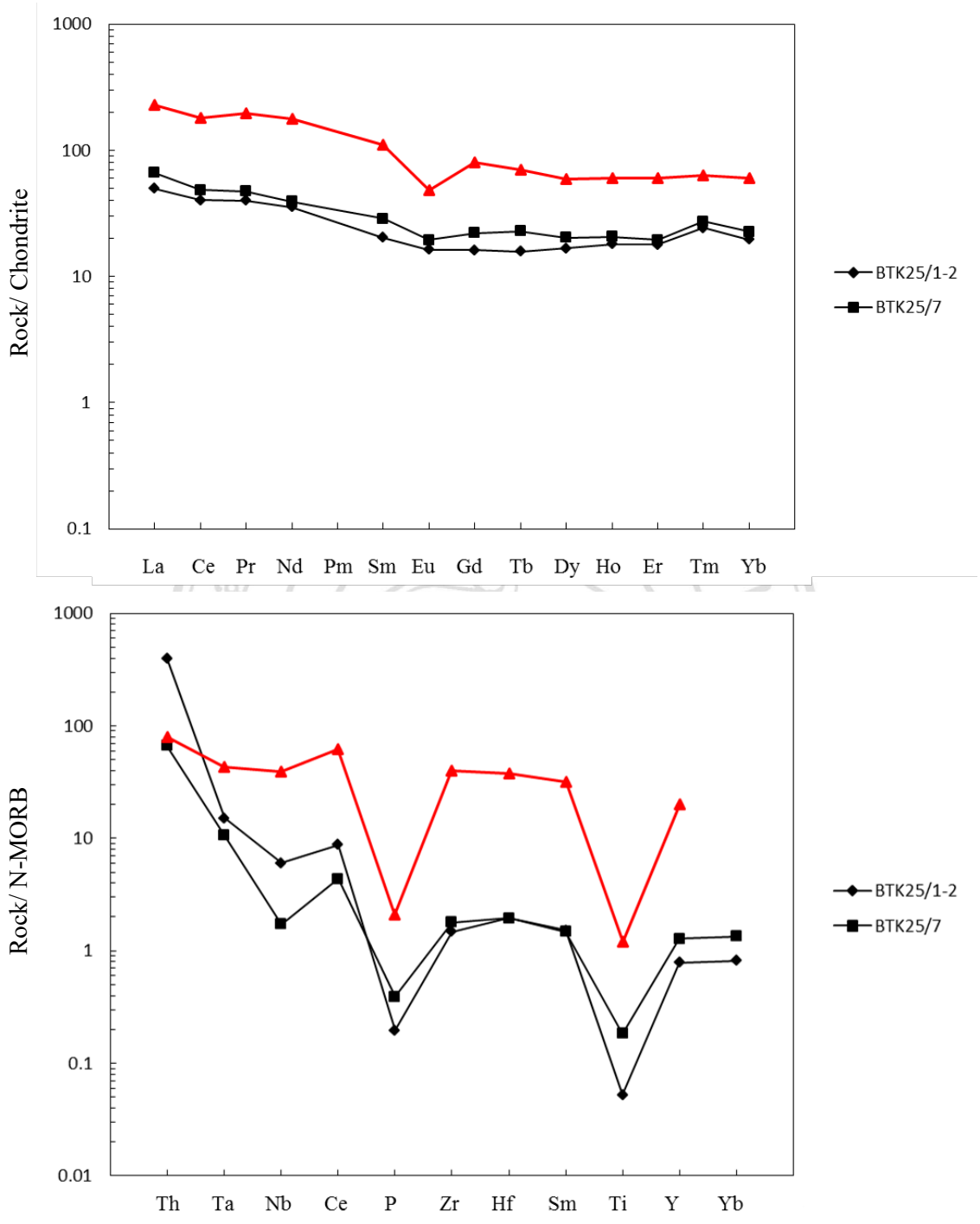

Figure 4.20 Chondrite-normalized REE patterns (a) and N-MORB normalized multi-element patterns (b) for the studied, least-altered volcanic and associated rocks of Group I and their modern analogue; Miocene intra-plate A2-type rhyolites (red symbol) from Jabal Shama, Saudi Arabia (Surour *et al.,* 2016). Chondrite-normalized values are those of Taylor and Gorton (1977) and N-MORB normalized values are those of Sun and McDonough (1989).

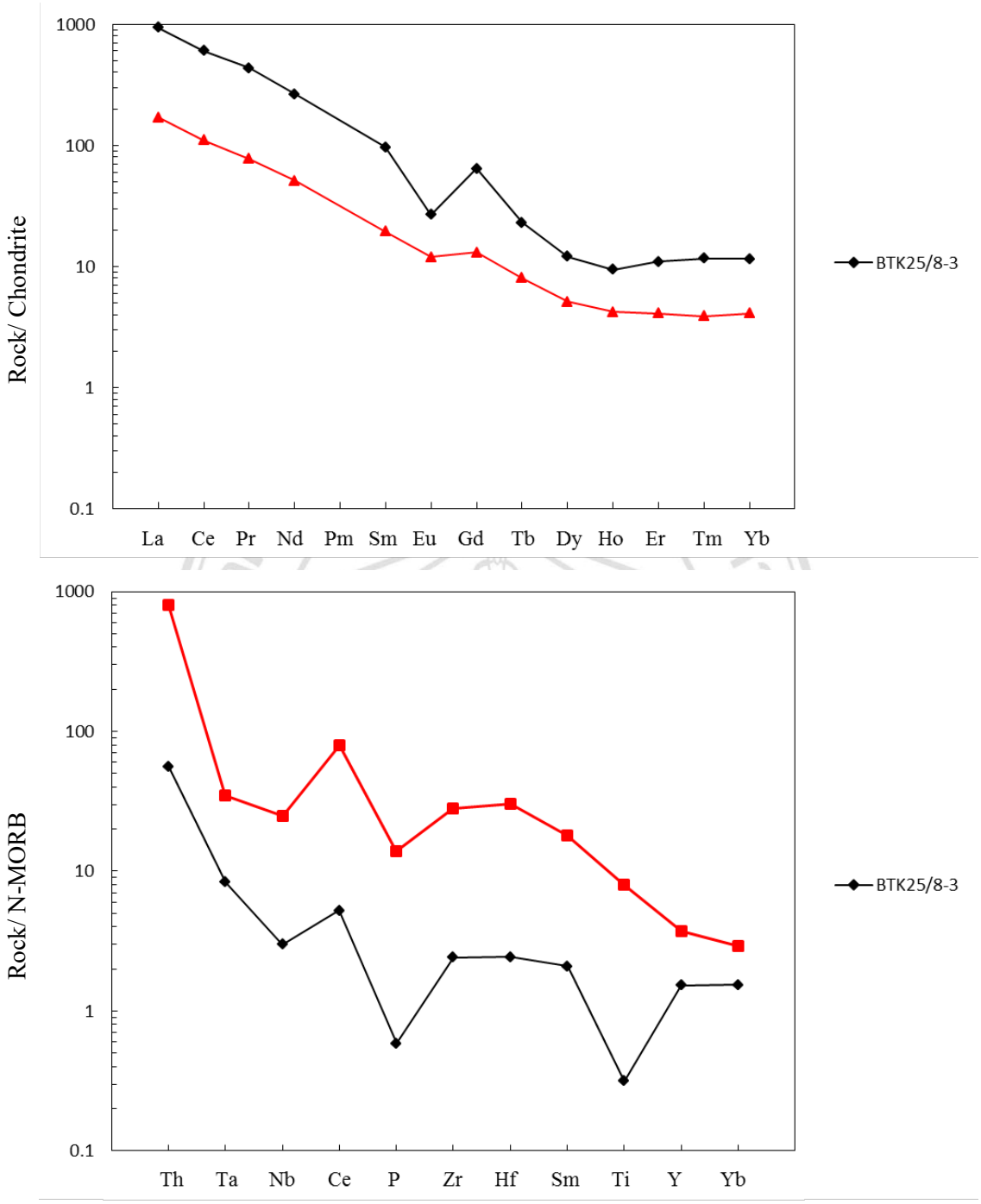

Figure 4.21 Chondrite-normalized REE patterns (a) and N-MORB normalized multi-element patterns (b) for the studied, least-altered volcanic and associated rocks of Group II and their modern analogue; Miocene basaltic dike (red symbol) from Miocene magmatism in the Yaguila-Sharang district, Tibet (Zhao *et al.,* 2016). Chondrite-normalized values are those of Taylor and Gorton (1977) and N-MORB normalized values are those of Sun and McDonough (1989).

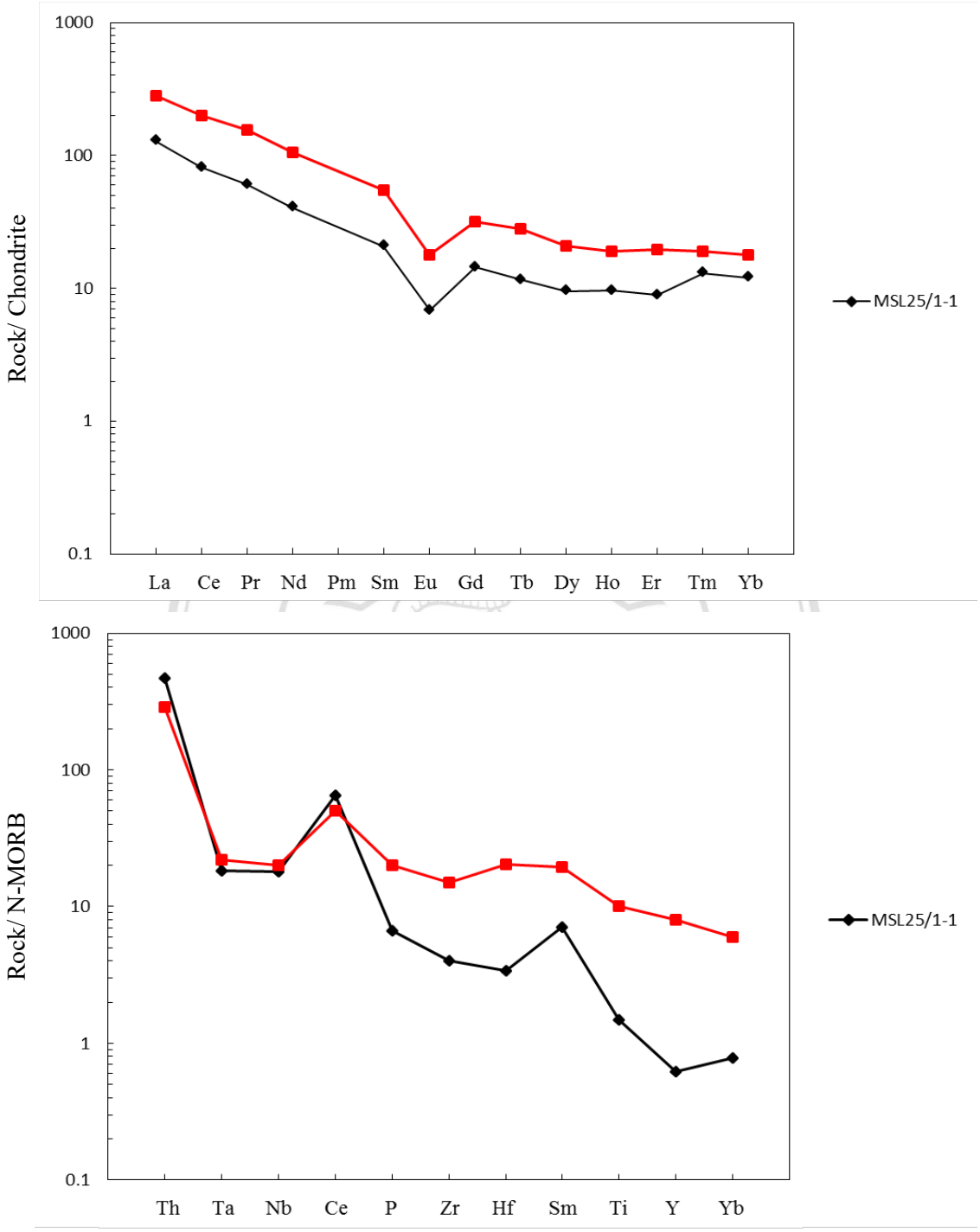

Figure 4.22 Chondrite-normalized REE patterns (a) and N-MORB normalized multi-element patterns (b) for the studied, least-altered volcanic and associated rocks of Group III and their modern analogue; Miocene rhyolite porphyry (red symbol) from Miocene magmatism at Yaguila, Tibet (Zhao *et al.,* 2016). Chondrite-normalized values are those of Taylor and Gorton (1977) and N-MORB normalized values are those of Sun and McDonough (1989).

Sharang Miocene dikes (~30–10 Ma), suggesting they were both generated from melting of enriched lithospheric mantle.

The representative of the Group IV rocks is most comparable in chemical composition with the basalt from the Karoo volcanic rocks in the southern Lebombo monocline, Mozambique, South Africa, which have been formed as a within-plate in south-eastern Africa (Melluso *et al.,* 2008) (Figure 4.23). The Karoo volcanic sequence in the southern Lebombo monocline in Mozambique contains different silicic units in the form of pyroclastic rocks, and two different basalt types (Cretaceous). The collision produced strong rifting (Baragoian-Barsaloian) especially in N-S dextral shear zones over 100 km east of the West Pokot suture, north central Kenya. The shear zones are associated with late Barsaloian within-plate granites.

The representatives of the Group V rocks are chemically similar to the Quaternary basalt from the Jaŕan volcanic valley, Central Volcanic Zone in Southern Peru (Gałaś*,* 2014) (Figure 4.24). The Quaternary Andahua volcanic group is located within the Central Volcanic Zone in Southern Peru, which have been formed as an active continental margin in the central Andes. The Andahua volcanic group is made up of trachyandesites, basaltic trachyandesites and dacites. The phenocrysts are represented mainly by plagioclase, but olivine, clinopyroxene and hornblende are also present. Their basaltic parental magmas were enriched in fluids derived from dehydration of the subducted oceanic crust.

The representative of the Group VI rocks is most comparable in chemical composition with the Late Miocene Topaz-bearing rhyolite from the Chivinar volcano, in Central Andes, NW Argentina, which have been formed as a back arc setting in the eastern Andes (Gioncada *et al.,* 2014) (Figure 4.25). Topaz-bearing rhyolite lavas were erupted as domes and cryptodomes during the early history of the Late Miocene Chivinar volcano, in Central Andes. The extensional regime due to the presence of the transtensive Calama-Olocapato-El Toro (COT) structure suggests a correspondence with topaz rhyolites in North America and China, sharing similar geochemical features unrelated to subduction, and, thus highlights

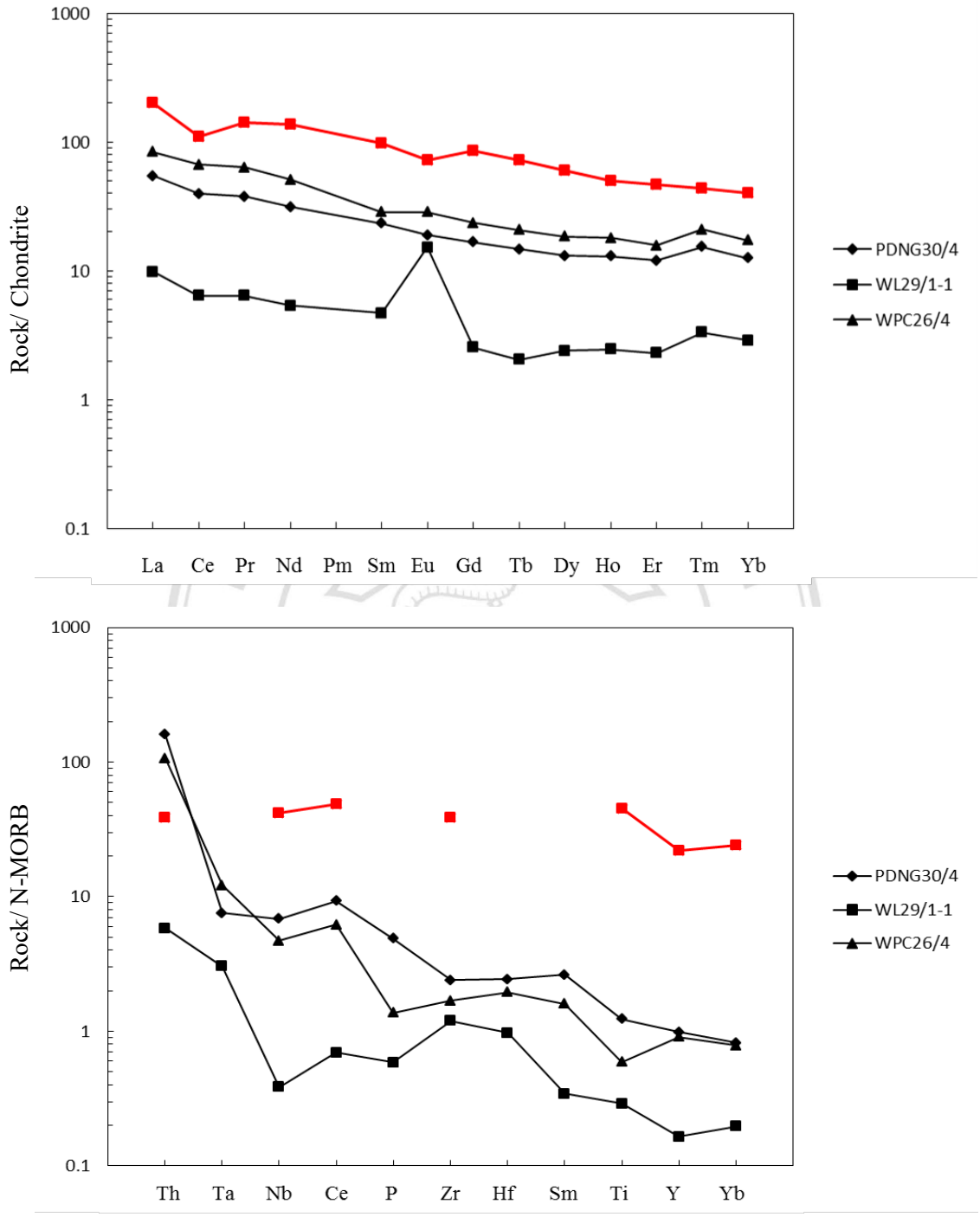

Figure 4.23 Chondrite-normalized REE patterns (a) and N-MORB normalized multi-element patterns (b) for the studied, least-altered volcanic and associated rocks of Group IV and their modern analogue; basalt (red symbol) from the Karoo volcanic rocks in the southern Lebombo monocline, Mozambique ,South Africa (Melluso *et al.,* 2008). Chondrite-normalized values are those of Taylor and Gorton (1977) and N-MORB normalized values are those of Sun and McDonough (1989).

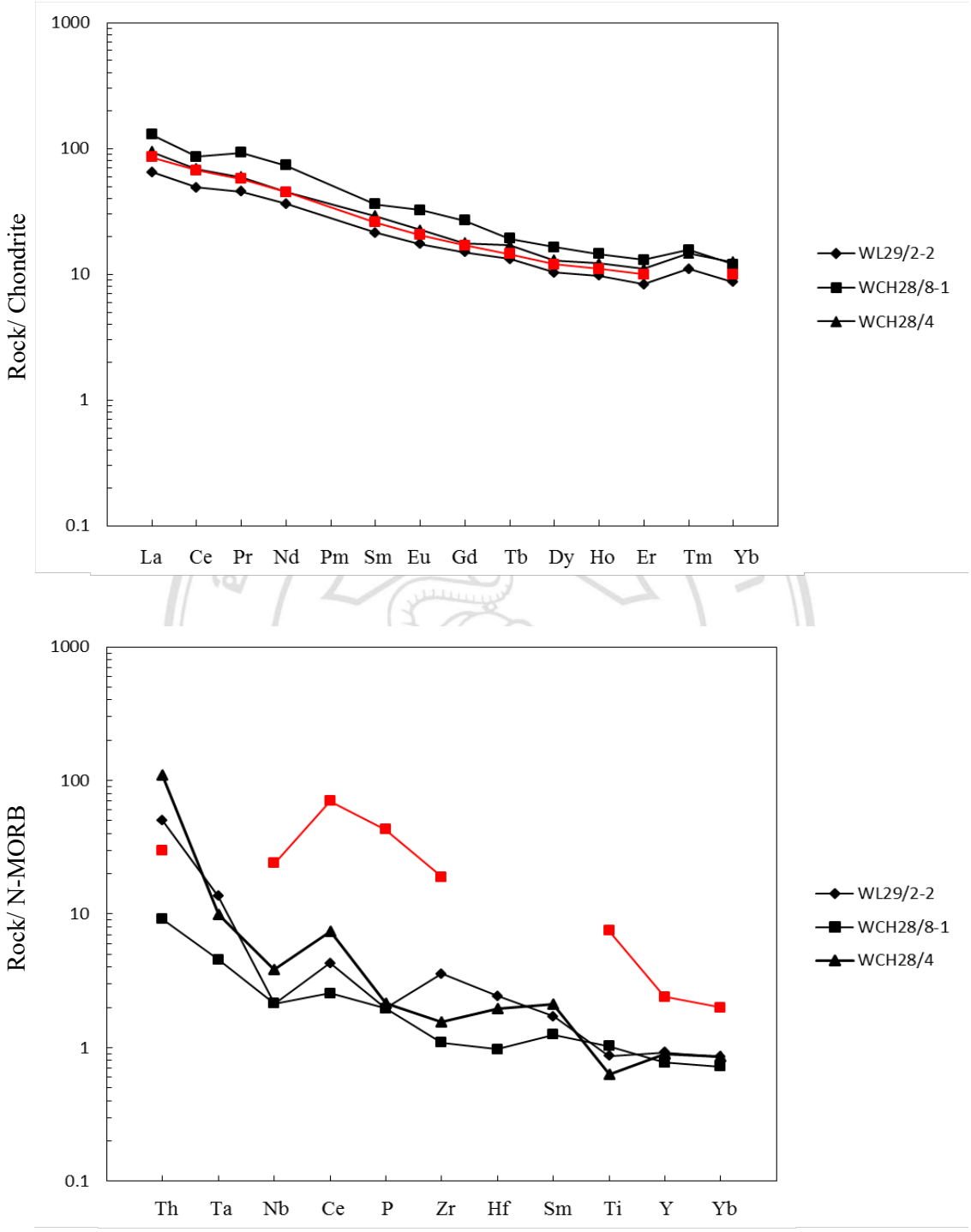

Figure 4.24 Chondrite-normalized REE patterns (a) and N-MORB normalized multi-element patterns (b) for the studied, least-altered volcanic and associated rocks of Group V and their modern analogue; Quaternary basalt (red symbol) from the Jaŕan volcanic valley, Central Volcanic Zone in Southern Peru (Gałaś, 2014). Chondrite-normalized values are those of Taylor and Gorton (1977) and N-MORB normalized values are those of Sun and McDonough (1989).

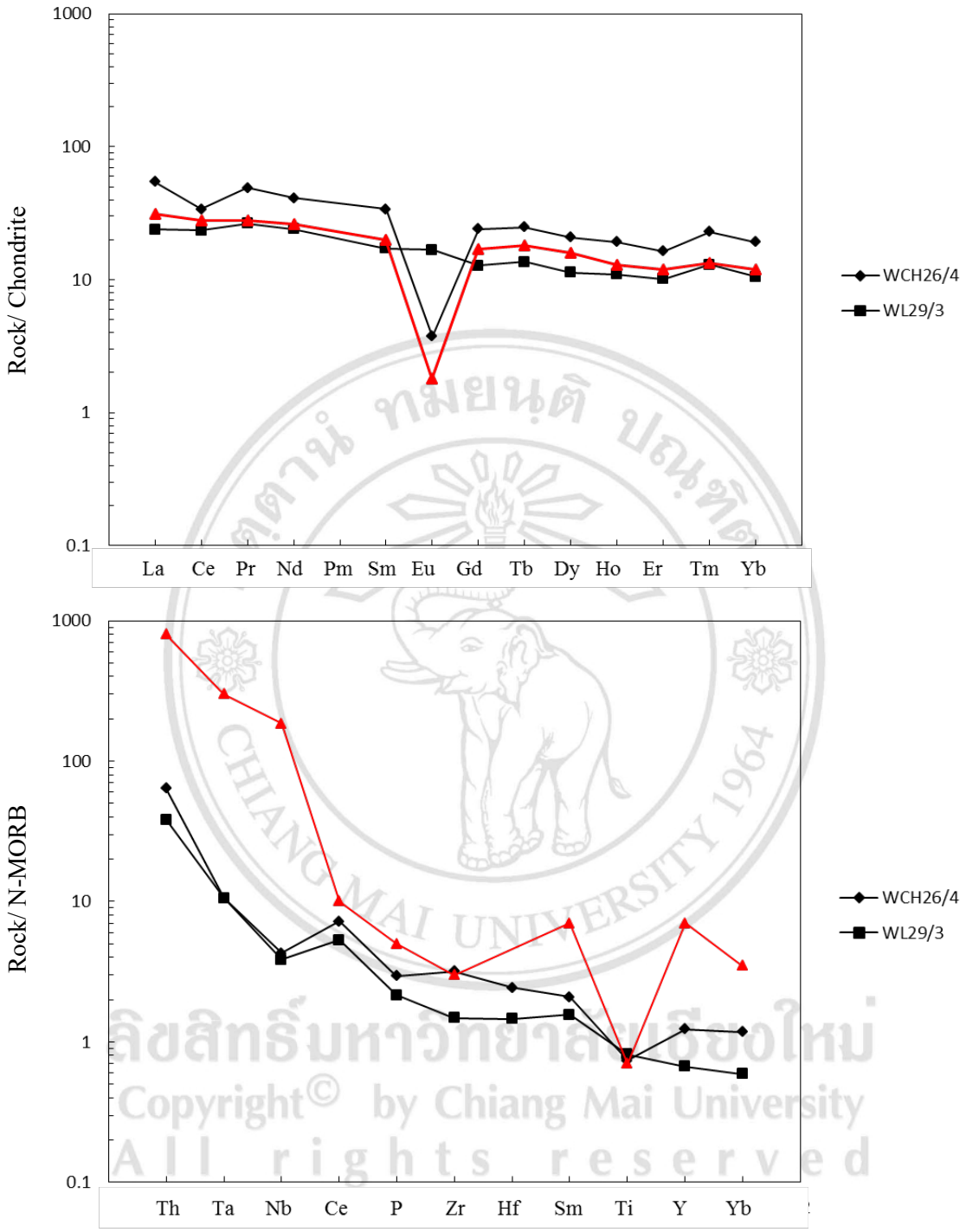

Figure 4.25 Chondrite-normalized REE patterns (a) and N-MORB normalized multi-element patterns (b) for the studied, least-altered volcanic and associated rocks of Group VI and their modern analogue; Late Miocene Topaz-bearing rhyolite (red symbol) from the Chivinar volcano, in Central Andes, NW Argentina (Gioncada *et al.,* 2014). Chondrite-normalized values are those of Taylor and Gorton (1977) and N-MORB normalized values are those of Sun and McDonough (1989).

preferred conditions for the formation of magmatic topaz in overall intraplate settings.

The Group VII rocks are closely similar in chemical composition to Quaternary Aphyric high-K andesite from the Andes, Ollagüe volcano region, which have been formed as an active continental margin in the central Andes (Mattioli *et al.,* 2006) (Figure 4.26). The SC2 incompatible trace element pattern has a typical arc-like signature with Sr–Nd isotopic ratios falling within the range of the Quaternary volcanic rocks of the CVZ, straddling between the less contaminated basaltic andesites and the more contaminated intermediate to acid extrusives of the Ollagüe volcano that is located in El Loa Province, Antofagasta Region, Chile and is the part of Andes mountain range (Singtuen and Phajuy, 2016).

The representatives of the Group VIII rocks are chemically similar to the Miocene within-plate rhyolite from the Karoo volcanic rocks in the southern Lebombo monocline, Mozambique, South Africa, which have been formed as a within-plate in south-eastern Africa (Melluso *et al.,* 2008) (Figure 4.27). The collision produced strong within-plate deformation (Baragoian-Barsaloian) especially in N-S dextral shear zones over 100 km east of the West Pokot suture, north central Kenya. The shear zones are associated with late Barsaloian within-plate granites (Late Cretaceous).

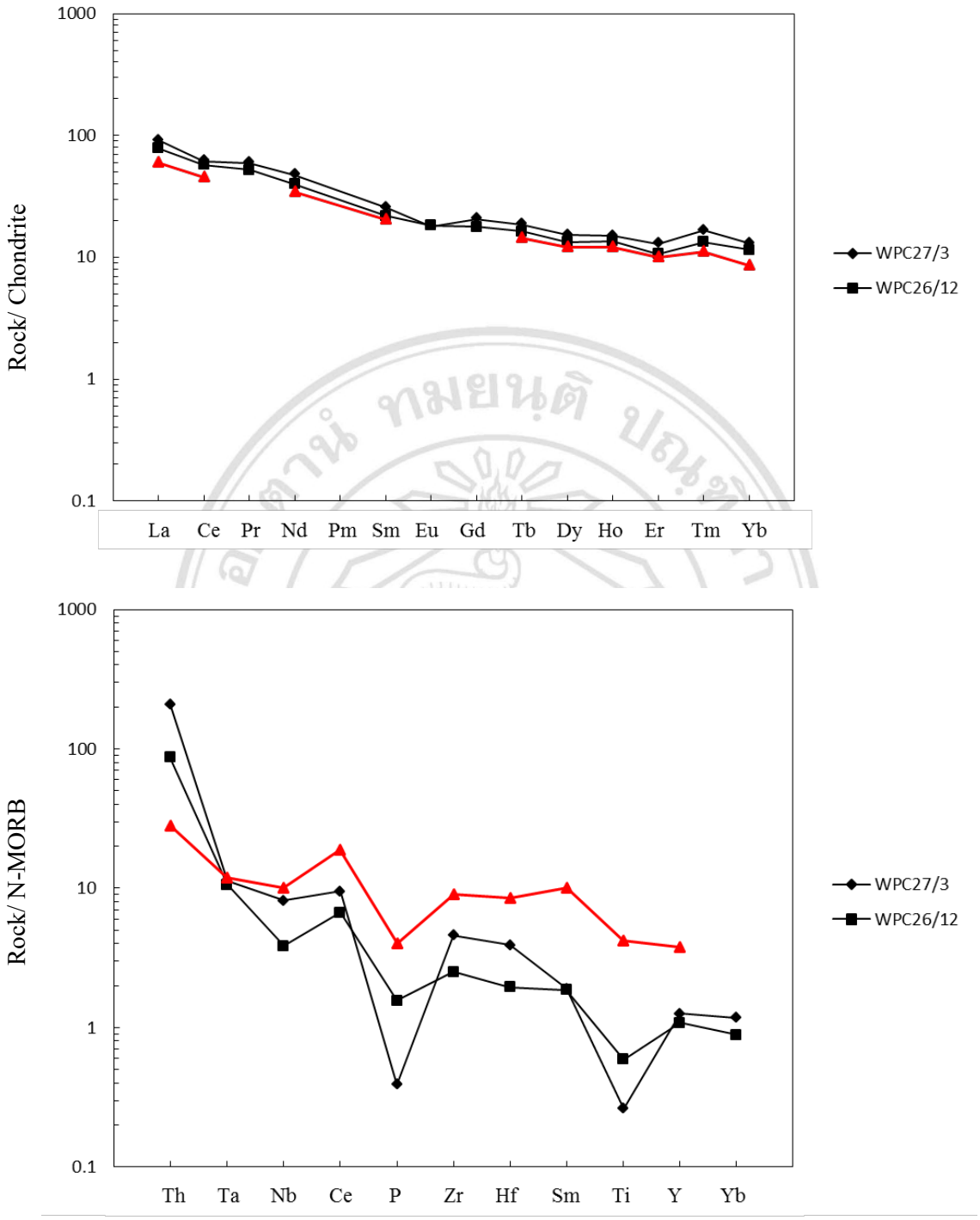

Figure 4.26 Chondrite-normalized REE patterns (a) and N-MORB normalized multi-element patterns (b) for the studied, least-altered volcanic and associated rocks of Group VII and their modern analogue; Quaternary Aphyric high-K andesite (red symbol) from the Andes, Ollagüe volcano region (Mattioli *et al.,* 2006). Chondrite-normalized values are those of Taylor and Gorton (1977) and N-MORB normalized values are those of Sun and McDonough (1989).

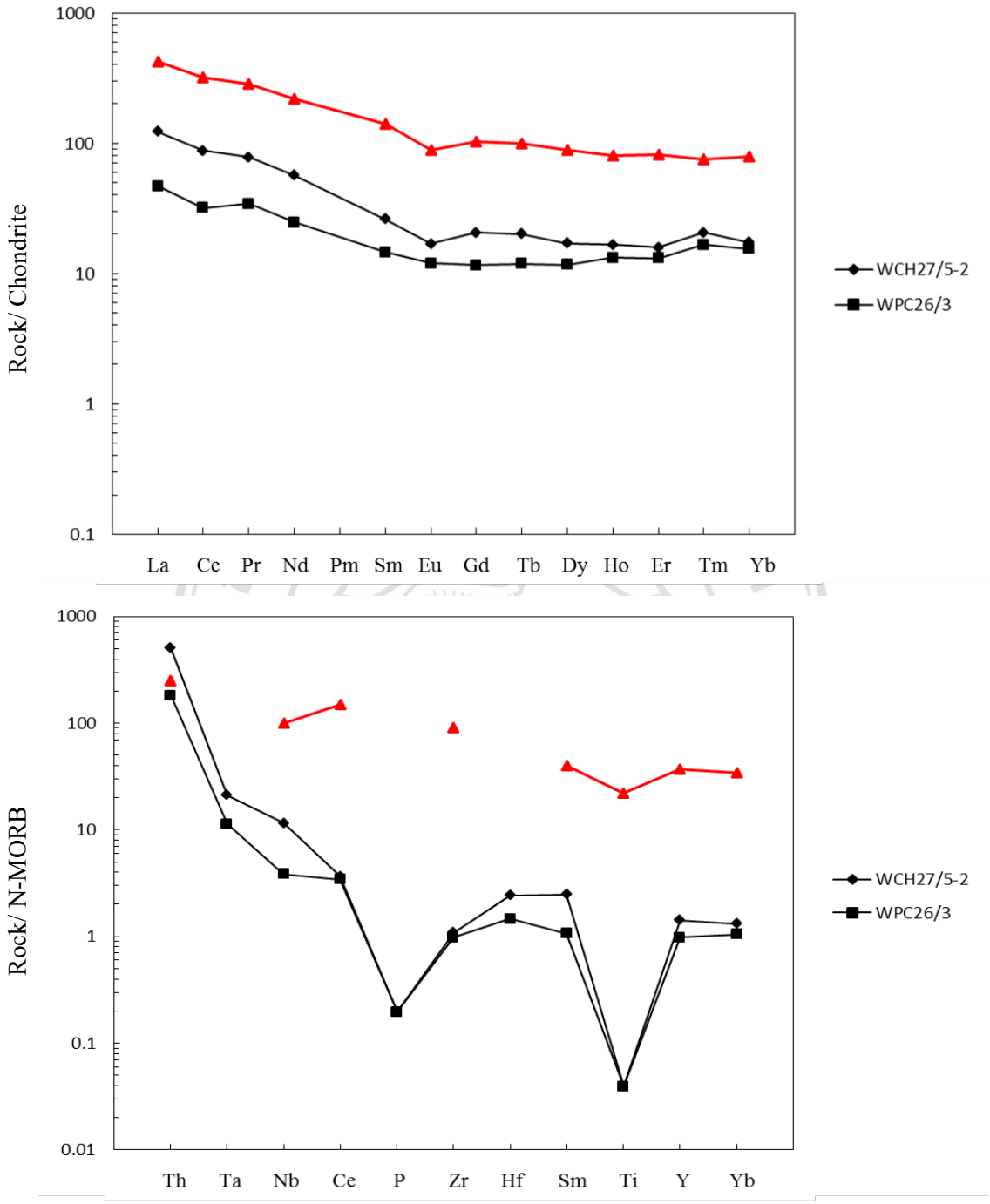

Figure 4.27 Chondrite-normalized REE patterns (a) and N-MORB normalized multi-element patterns (b) for the studied, least-altered volcanic and associated rocks of Group VIII and their modern analogue; Miocene within-plate rhyolite (red symbol) from the Karoo volcanic rocks in the southern Lebombo monocline, Mozambique ,South Africa (Melluso *et al.,* 2008). Chondrite-normalized values are those of Taylor and Gorton (1977) and N-MORB normalized values are those of Sun and McDonough (1989).